



UTRECHT UNIVERSITY

CLIMATE PHYSICS

INSTITUTE FOR MARINE AND ATMOSPHERIC RESEARCH

Master thesis

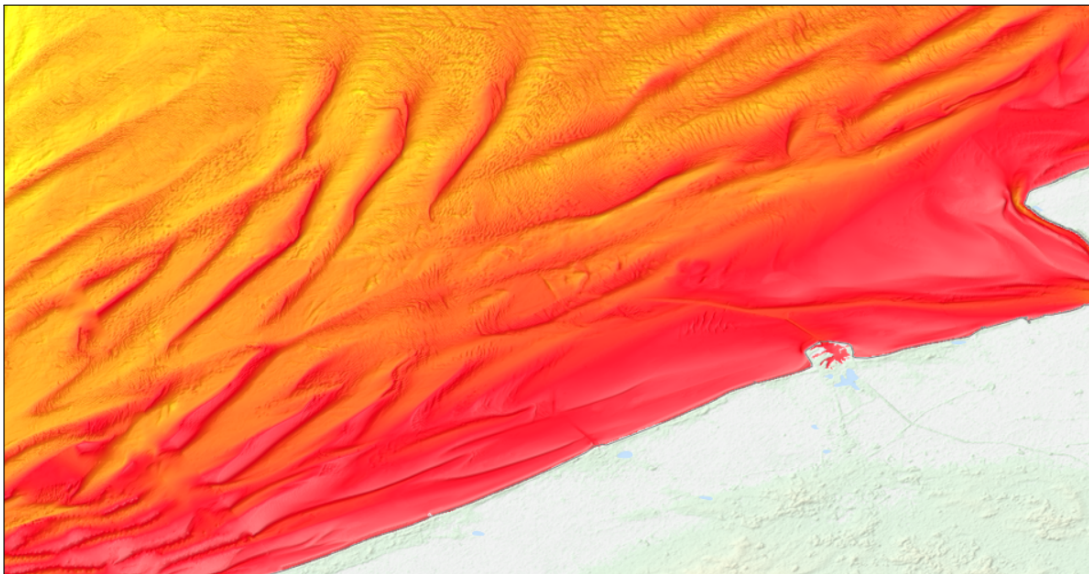
**Modelling shelf morphodynamics and shoreline
change: free behaviour and response to the
construction of artificial islands**

Author:

THOM WOLF
4212398

Supervisors:

PROF. DR. H.E. DE SWART
& DR. A. NNAFIE



January 11, 2019

Abstract

An option to protect coasts from erosion and flooding caused by sea level and changes in the wave climate, is the construction of offshore artificial islands. It is however unknown how precisely these islands would affect the coast. This study investigates the natural hydro- and morphodynamics of a mesotidal coastal zone and its response to the presence of offshore artificial islands.

To this end, the coupled Delft3D-SWAN numerical model is used, which accounts for tides, waves, sand transport and bed level update. An idealized rectangular model domain of 55 by 50 km is considered, which crudely mimics the Belgian continental shelf. A grid size of 700 m is used, hence processes in the nearshore zone are not explicitly resolved. Instead, from the wave conditions, the CERC formula is used to calculate longshore sand transport in the breaker zone and the resulting accretion/erosion of the shoreline is determined. The natural behaviour of the continental shelf is studied by conducting spin-up runs for a period of 1000 years, starting from an initially linear bottom profile in the cross-shore direction. Subsequently, one or more islands are created and the response of the system to these perturbations is studied.

This study shows for the first time, using a full process-based morphodynamic model the formation of mature tidal sand ridges on a shelf with a sloping bottom. The construction of an island affects the growth of the sand ridges and gives rise to accretion of the coastline behind the island and erosion further downstream, however the net change of the coastline is small. The shelf area in which the bed level is influenced by an island increases when an island is placed further offshore, decreases (normalized by the island area) when it has a longer alongshore length or when the number of adjacent islands increases. Computed coastal accretion and erosion rates decrease when islands are placed further offshore, though the net rate increases. For an increasing island size, accretion and erosion rates increase, but the net remains zero. In the case of two islands, separated by an inlet, accretion and erosion rates increase for wider inlets, but this increase is minimum once the width is larger than 5 km.

Abstract for laymen

This Master thesis is about understanding how tides and waves shape the bottom of coastal seas, how they determine the position of the coastlines and how these processes are influenced by human interventions. This topic is called coastal morphodynamics and the systems studied are called coastal systems.

Coastal seas are relative shallow bodies of water that extend from the shoreline till the shelf break, where a steep slope indicates the transition towards the deep ocean. From the shelf break till the shoreline, a coastal sea consist of multiple subsequent zones. These are the outer shelf, the inner shelf, the nearshore zone and the surf zone (figure 1). These zones distinguish themselves by their different transverse bottom slopes and different dominant hydrodynamic processes. The outer shelf has a small transverse bottom slope, which becomes larger (order of $\sim 10^{-3}$ m/m) at the inner shelf. Due to the water depth becoming shallower, the hydrodynamics here become less geostrophic. The transition of the inner shelf towards the nearshore zone is marked by the wave base, which is the depth at which waves under normal conditions begin to interact with the seabed. In the nearshore zone, the transverse bottom slope has increased to a value in the order of $\sim 10^{-2}$ m/m. It is a dynamic environment where many processes are related to changes in wave characteristics (i.e. increasing wave height and change of wave direction). Shoreward of the nearshore zone is the surfzone, which extends to the coastline. Here waves break as they propagate shoreward into shallower water.

Various studies (see Ribas et al. (2015) for a review) have demonstrated that in coastal seas, the natural interactions between tide and wind driven currents, waves and the sandy bed of a shelf result in different rhythmic bedforms. The latter include the large scale (order of kilometres) tidal sand ridges and shoreface-connected ridges, the mesoscale (order of hundreds of meters) tidal sand waves and the smaller scale (order of meters, centimeters) bedforms like megaripples and ripples. All these bedforms grow on different timescales. For instance tidal sand ridges have time scales in the order of hundreds of years, while smaller bedforms may grow on hourly to yearly time scales. The described large scale bedforms are found on the outer and inner shelf, whereas the smaller scale bedforms are found in the shallower parts of the coastal zone.

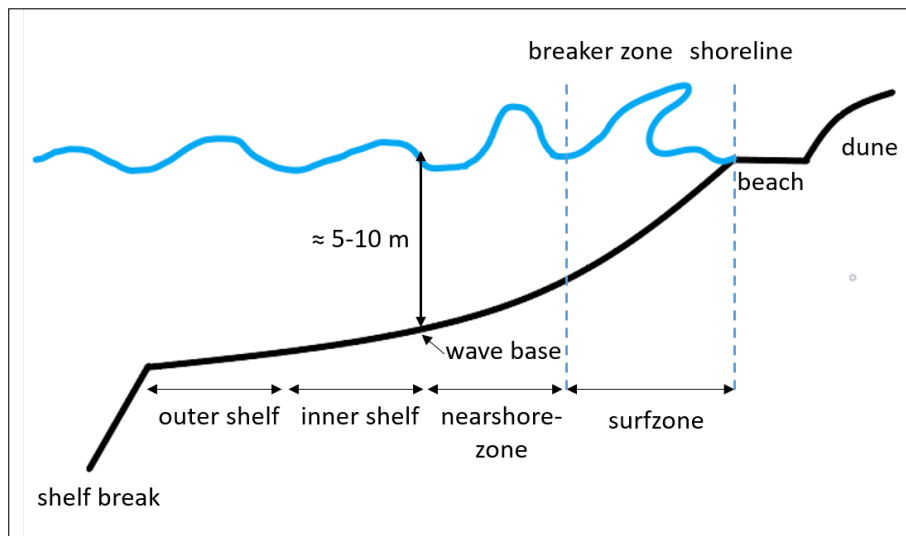


Figure 1: Schematized overview of coastal zone.

In general, studying coastal systems is relevant since about 40 % of the world's population lives within a 100 km distance from a coast (Crossland et al., 2005). Also, in 2010, 8 of the top 10 largest cities in the world were located at the coast. Therefore, protection of coastal lowlands from flooding is crucial. Furthermore, coastal seas are increasingly used as navigation routes for ships transporting goods, are interesting locations for upcoming wind farms, important for tourism and are of significant ecological value as they provide a habitat for many marine species. To be able to continue to live in and utilize these coastal areas, while keeping an eye on the ecology, proper coastal zone management is needed. In particular, management of the coast requires knowledge about the response of coastal systems to sudden events (e.g. storm surges), to human interventions (e.g. dredging, construction work offshore or at the coast) and to changes that occur on time scales of decades to centuries (e.g. sea level rise (SLR)). Observations indicate a current SLR of 2 mm/year, but due to human activities this is foreseen to accelerate in the near future (IPCC, 2014).

With regards to coastal protection, several measures have been implemented or are proposed (figure 2a), varying from hard engineering constructions (e.g. concrete seawalls and groynes) to soft measures using sand, like beach and shoreface nourishments (dumping sand, which is excavated from the sea bed far offshore, on the beach or near the shore). Also a mega nourishment like the Dutch Sand Engine (figure 2b), where on the coast a peninsula of sand is created extending one kilometer into the sea, is based on the philosophy of 'building with nature' by using sand instead of concrete. Another potential measure to protect the coast, concerns the construction of sandy artificial islands offshore of coastal areas. The idea behind this measure is that the area between the islands and the shoreline will be sheltered from shoreward propagating waves, thereby reducing shoreline erosion while also giving rise to accretion of sediment in this area resulting in the formation of shallow lagoons. Ideas for constructing such artificial offshore islands exist for instance in the Netherlands, Belgium and the US (e.g. Emergo ¹, Complex project kustvisie², Keenan and Weisz (2017)).

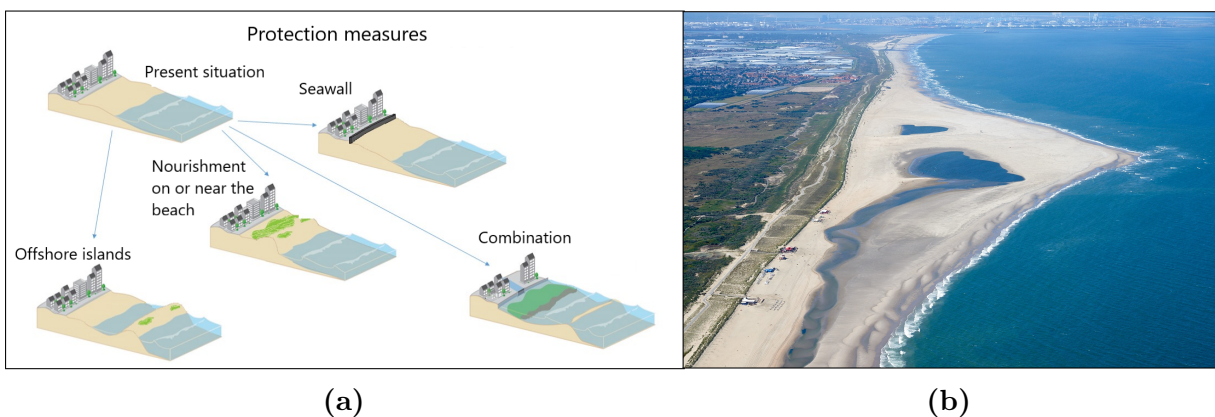


Figure 2: (a) Schematized overview of possible coastal protection measures, including beach and shoreface nourishments, island construction, seawall construction or a combination (hard and soft). Adapted from the Complex project Kustvisie (2017). (b) The Dutch Sand Engine³ (Large nourishment project near the Hague, the Netherlands).

For understanding the effects of measures on the coastal system, first deep knowledge is required about natural dynamics of coastal systems (i.e. without changes). This knowledge

¹<http://www.springtij.nu/emergo/>

²<http://www.kustvisie.be>

³<https://www.dezandmotor.nl>

is gained along three different lines: by collecting and analysing field data, by studying the coastal system using complex models and by studying the coastal system using schematised models. Here, complex models encompass many physical processes and are used for detailed short term predictions, whereas schematised models encompass less physical processes and are used to gain fundamental insight into the role of the individual physical processes in a system.

The study in this thesis will address, while using a schematised modelling approach, the morphodynamics of a sandy coastal system that mimics the Belgian coastal zone when sandy offshore artificial islands are implemented on the shelf. The main objectives are:

1. Quantifying the natural behaviour of bottom shapes on the shelf and the coastline
2. As in (1), but quantifying the effect of constructing artificial islands on the shelf
3. Understanding both the natural behaviour and the response of the shelf and the coastline to the intervention of constructing artificial islands

For answering these questions, the schematized model used distinguishes between the shelf (outer and inner), the nearshore zone and the surf zone (figure 1). On the shelf, a numerical morphodynamic model is used, called Delft3D-SWAN. It solves waves, depth averaged currents, sand transport and bottom changes. In the nearshore zone, waves are computed by applying linear wave theory on the wave results of the Delft3d-SWAN model. In this computation, the position of the breaker line is determined as well as the wave characteristics at the breaker line. The latter information is now used to calculate longshore sand transport in the surf zone. Gradients in that transport will cause changes in the coastline, associated with beach erosion or beach accretion.

In this study, it is found that, when using the numerical morphodynamic Delft3D-SWAN model, mature tidal sand ridges are formed on the shelf. Their patterns, growth and migration can be explained with the classical theory of [Huthnance \(1982a\)](#). These ridges have a profound impact on the dynamics of the surf zone, by creating peaks in the accretion and erosion of the coastline with values in the order of several meters per year.

When implementing an island on the shelf, it is found that there is initially strong erosion of sand at one island tip. In the direct vicinity of the island, the characteristics and migration of the tidal sand ridges on the shelf are significantly altered, whereas the shelf further offshore undergoes less change. Also, a shadow zone is created shoreward of the island, where the wave height is dampened. This gives rise to accretion of the coast behind the island and erosion further downstream, however the net change of the coastline remains almost unchanged.

By studying different island configurations, it is found that the area in which the bed level is influenced by an island increases when an island is placed further offshore. Normalized by the island area, the area in which the bed level is influenced by an island, decreases when an island has a longer alongshore length and also decreases for an increasing number of adjacent islands. The variance in coastline accretion/erosion rates in the model domain decreases when islands are placed further offshore, though the small net accretion rate increases. For an increasing island size, the variance in coastline accretion/erosion rate increases, but the net accretion remains almost zero. In the case of two islands, separated by an inlet, variance in accretion/erosion rates increases for wider inlets, but the increase is minimal once the width is larger than 5 km. The net accretion rate remains very small for all inlet cases.

Contents

1	Introduction	6
2	Material and methods	7
2.1	Coastal zone model geometry	7
2.2	Shelf model: Delft3D and SWAN	8
2.3	Nearshore model: longshore sand transport and coastline changes	8
2.4	Default setting and numerical aspects	9
2.5	Design of experiments	12
2.5.1	Natural behaviour	12
2.5.2	Default island case	12
2.5.3	Sensitivity experiments: different island configurations	12
2.6	Methods for analyzing results	13
3	Results	13
3.1	Natural behaviour	13
3.2	Presence of islands: default case	16
3.3	Different island configurations	19
3.3.1	Island distance to coastline	19
3.3.2	Island size (varying alongshore length)	21
3.3.3	Multiple islands	22
3.3.4	Variable inlet width	22
4	Discussion	23
4.1	Physical analysis	23
4.1.1	Natural behaviour: formation tidal sand ridges	23
4.1.2	Default island: residual currents and sand transport on shelf	24
4.1.3	Shoreline change: effect of multiple wave conditions	25
4.1.4	Sand volume budget of domain	26
4.2	Sensitivity analysis	26
4.2.1	Numerical parameters	26
4.2.2	Sand transport equation	26
4.3	Physical limitations	26
5	Conclusions	27

1 Introduction

Many low-lying coastal areas around the world experience beach erosion and flooding to the ongoing rise in mean sea level and changes in wave and storm climate. This poses a threat to safety of humans living in these areas. To protect such coasts, several measures have been implemented to maintain coastal areas, varying from hard engineering constructions (e.g. seawalls) to soft measures like beach and shoreface nourishments (Hanson et al., 2002). Also mega nourishments like the Dutch Sand Engine (Van Slobbe et al., 2013) have been executed that are based on the philosophy of building with nature. However, these interventions can have potentially negative impacts on the natural dynamics of a sandy coastal system. To assess these effects, systematic studies with process based models are required.

Regarding interventions on the shelf, many studies focused on their impacts on large scale bottom patterns (i.e. tidal sand ridges (Dyer and Huntley, 1999)). Roos et al. (2008) investigated the hydrodynamic effects and morphodynamic impact of large-scale offshore sand extraction (on a flat bed) for a variety of pit designs using a process-based idealized model. They found that sandpits trigger the morphodynamic instability associated with the formation tidal sand ridges and that the model results depend on the pit geometry. Nnafie et al. (2014) investigated the response of shoreface-connected sand ridges to the extraction of sand, using a process based model. They determined, for multiple sand extraction scenarios, the response timescales of the ridges and new equilibrium states.

A modelling study regarding larges scale interventions in the surf zone by Luijendijk et al. (2017) investigated the initial changes in longshore sediment transport and morphology due to the Sand Engine. They found intense erosion of the Sand Engine occurring for individual high energy wave events and accretion of sand along adjacent north and south coastlines. The long-term diffusion and feeding capability of the Sand Engine was studied by Arriage et al. (2017). They found that the Sand Engine will display diffusive behaviour, caused by asymmetric feeding of sand to the adjacent beaches and that its centre of mass will slowly migrate.

Another measure to protect the coast, concerns the construction of artificial islands offshore of coastal areas (e.g. Complex project kustvisie⁴ and Keenan and Weisz (2017)). However, the specific impact of such islands on the hydrodynamics (waves, tides), the morphology and the shoreline is not known.

These considerations motivate the three specific research questions, which form the base of this study.

1. What is the natural (without islands) morphodynamic behaviour of a shelf with a sloping bottom and the resulting shoreline response?
2. What is the quantitative impact of the presence of artificial islands in front of a sandy coast on the (a) morphodynamics of the shelf and (b) longshore sand transport in the surf zone and related coastline accretion and erosion. How do these depend on the design of the islands (number, length, distance to the coast)?
3. What are the physical processes that control the response of a coastal system to the construction of artificial islands?

These questions are addressed by conducting experiments with a numerical morphodynamic model which solves waves, depth averaged currents, sand transport and bottom

⁴<http://www.kustvisie.be>

changes. A rectangular model domain is considered, that roughly mimicks the Belgian sandy shelf. From the output of the model, the longshore sand transport in the surf zone is calculated with the CERC formula and the resulting coastal accretion/erosion follows from application of a one-line model (Komar, 1998; Falqués and Calvete, 2005).

A description of the model components is given in sections 2.1 till 2.3. In section 2.4 till 2.6 the model setup, design of experiments and tools to analyse the model output data are discussed. The model results are presented in section 3 and discussed in section 4. Section 5 contains the conclusions.

2 Material and methods

2.1 Coastal zone model geometry

In this study, the coastal zone is captured with two model domains, an idealized rectangular shelf domain (size: $L_x \times L_y$) which lies a few kilometres offshore (figure 3a) and a shoreward adjacent nearshore zone domain (figure 3b). Here x and y are the cross-shore and alongshore coordinates, respectively and z is the vertical coordinate.

The shoreward boundary $x = L_x$ of the shelf domain, represents the transition between the inner shelf and the nearshore zone. The mean sea level is at $z = 0$ and the bed level is at $z = z_b$. The initial bathymetry of the shelf is represented by an alongshore uniform linear sloping bed profile $z_b(x, y, t) = -D(x, y, t) = -D_0(x) = D_{sea} - \beta x$, where D is the depth, D_0 the initial depth at $t = 0$, D_{sea} its value at the seaward boundary and β a constant slope. The depth D_{L_x} is finite at the shoreward boundary. Bottom perturbations with respect to the reference bed $z_b(x, y, t) = -D(x, y, t)$ are denoted as $h(x, y, t)$.

The nearshore zone domain lies shoreward adjacent to the shelf domain, having an equal alongshore length L_y and shore parallel depth contours ranging from $D(x = L_x, y, t) = D_0(L_x) = D_{L_x}$ to the coastline where $D = 0$. General information about the shelf and nearshore zone models is given in sections 2.2 and 2.3, respectively.

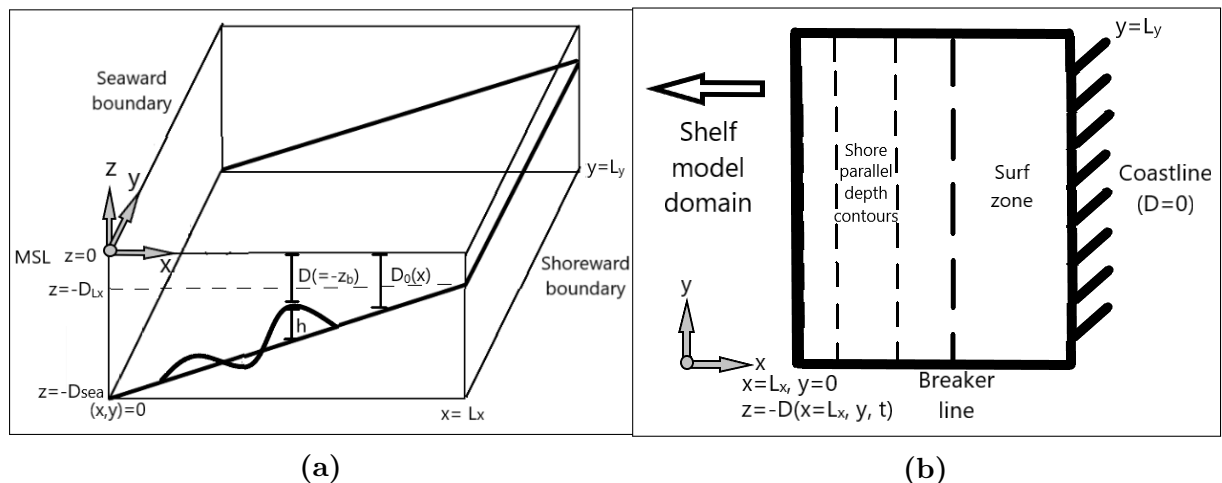


Figure 3: (a) Schematic overview of the shelf domain. For an explanation of the symbols, see the text. (b) Nearshore zone domain (top view). Here, the breaker line is the location at which wave breaking is most intense.

2.2 Shelf model: Delft3D and SWAN

The morphodynamics of the shelf is simulated with the coupled Delft3D-SWAN model (see figure 4). Delft3D (Lesser et al., 2004) is applied in its depth-averaged mode and it calculates currents (Delft3D-FLOW module), as well as, sand transport and bed evolution (Delft3D-MOR module), whilst SWAN (Booij et al., 1996) calculates the waves. Tides are affected by waves through enhanced bed shear stresses and introduced radiation stresses, whilst waves are influenced by currents (e.g. Doppler shift and depth changes due to tidal sea surface variations). Induced by currents and waves, the sand transport is computed with the formulation of Van Rijn (1993), which accounts for suspended and bedload transport. By modelling the flow in a depth-averaged mode, the offshore directed sand transport component due to waves (e.g. undertow) is not incorporated. Therefore, the onshore directed sand transport component due to waves is put to zero.

The change in bed level h over time is determined by the divergence in bedload transport and the exchange of suspended sediment between the water column and the bed.

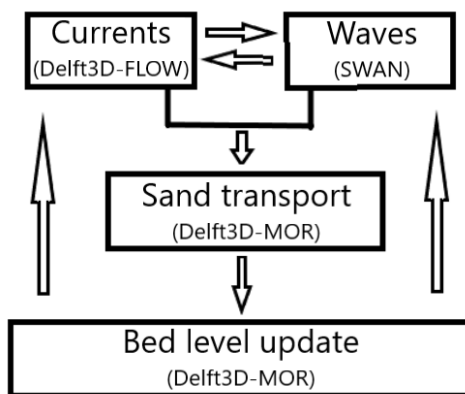


Figure 4: Delft3D-SWAN model overview

The currents in the Delft3D-FLOW model are described by the depth-averaged nonlinear shallow-water equations. At both the north and south (lateral) boundaries of the shelf domain, a Neumann water level gradient boundary condition is applied, based on the work of Roelvink and Walstra (2004). The seaward boundary is forced with water level conditions. For the shoreward boundary a free-slip condition is applied.

The SWAN wave model solves the spectral action balance equation, in this study used in its stationary form. Wave generation by wind and non-linear wave-wave interactions are not taken into account. At the lateral and seaward boundaries of the shelf domain, a JONSWAP wave spectrum is imposed. Waves are able to propagate through the shoreward boundary without being affected.

For the Delft3D-MOR module, at the lateral and seaward inflow boundaries, Neumann boundary conditions for sand concentrations are prescribed. At the shoreward boundary there is only a cross-shore diffusive sand transport q_x , due to the local bed slope $\partial D/\partial x$.

2.3 Nearshore model: longshore sand transport and coastline changes

In the nearshore domain, solely the over the surf zone integrated longshore volumetric sand transport Q_{vol} (in m^3s^{-1}) is computed from which its gradients are used to find initial coastline changes. Using the CERC formula (Shore Protection Manual, 1984; Komar, 1998), Q_{vol} is given as

$$Q_{vol} = \frac{KE_{br}c_{g,br} \sin(\theta_{br}) \cos(\theta_{br})}{(1-p)(\rho_s - \rho)g} \quad (1)$$

where, subscript *br* denotes variables at breaker line (location where wave breaking is most intense), K is an empirically determined calibration coefficient, p is the porosity factor, ρ_s and ρ are the sediment density and water density, respectively and g is the acceleration due to gravity. Furthermore, θ_{br} is the angle between wave propagation direction and shore normal direction, $c_{g,br} \approx \sqrt{gD_{br}}$ is the group velocity and $E_{br} = \frac{1}{16}\rho g H_{s,br}^2$ is the wave energy density, with $H_{s,br}$ is the significant wave height.

The accretion and erosion rates of the shoreline are determined by the alongshore gradients in Q_{vol} (Komar, 1998; Falqués and Calvete, 2005):

$$\frac{dx_s}{dt} = -\frac{1}{D_c} \frac{dQ_{vol}}{dy} \quad (2)$$

in which D_c is the depth of closure, x_s is the cross-shore shoreline position and y the alongshore position.

The knowledge of wave conditions needed for the CERC formula at the breaker line are provided by the output of the shelf model. However, since the shoreward boundary of the shelf domain is located seaward of the breaker line, the wave input variables for the CERC formula needed at the breaker line are not directly given by the shelf model output (figure 3b). To determine $H_{s,br}$, θ_{br} and D_{br} , the wave energy balance (without sources and sinks), the refraction equation and the dispersion relation assuming steady conditions and straight depth contours are solved for $x \geq L_x$ together with the criterion that at breaking $H_{s,br} = \gamma D_{br}$, with γ the depth induced breaking index.

2.4 Default setting and numerical aspects

As a prototype coastal area, the Belgian coastal area (figure 5) has been chosen. It is a prototype mesotidal sandy coastal system with ample observational tidal, wave and bathymetric data available. For the shelf domain, the experiment results are analyzed for a rectangular physical domain with a cross-shore width $L_x = 50$ km and a alongshore length $L_y = 55$ km, though computed on two separate (larger) rectangular computational domains (i.e. a Delft3D and a SWAN domain (figure 6)). The Delft3D domain has a size $L_{x,D} \times L_{y,D} = 50 \times 75$ km, while the SWAN domain has a size $L_{x,W} \times L_{y,W} = 75 \times 150$ km. The Delft3D domain is larger than the physical domain in order to exclude boundary effects in the physical domain, whilst the SWAN domain is larger in order to prevent wave shadow effects from affecting the results in the physical domain.

Motivated by the analysis of bathymetric data from the EMODnet Bathymetry website⁵, a linear depth profile from $D_0(x=0) = D_{sea} = 38.5$ m to $D_0(x=L_x) = 5$ m depth is chosen as initial bathymetry for the shelf domain, resulting in a bottom slope of $\beta = -6.7 \times 10^{-4}$ m. The Delft3D model domain is forced on the seaward and lateral boundaries with an astronomic semi-diurnal M2 tide having a tidal period of $T = 12.41$ h and amplitude of $\zeta = 1.8$ m travelling from south to north with a phase difference $\Delta\phi = 31.5^\circ$, based on harmonic analysis of water level data from buoys in the Belgian coastal region (i.e. Nieuwpoort, Vlaamsebanken⁶). Based on the wave analysis from another buoy (Deurloo⁷), JONSWAP wave spectra are imposed on the south and west boundaries of

⁵<http://www.emodnet-bathymetry.eu>

⁶<https://meetnetvlaamsebanken.be/map>

⁷<https://waterinfo.rws.nl>

the SWAN model domain with a significant wave height $H_s = 1$ m, direction $\theta = 220^\circ$ and a peak wave period $T_p = 6$ s.

For the nearshore domain, the results are also analyzed for a domain with length $L_y = 50$, equal to the length of the physical domain. A depth of closure D_c of 8 m is chosen (Hilton and Nicholls, 1998). The nearshore model uses H_s , θ and D results provided by the shelf model, at the shoreward boundary as input.

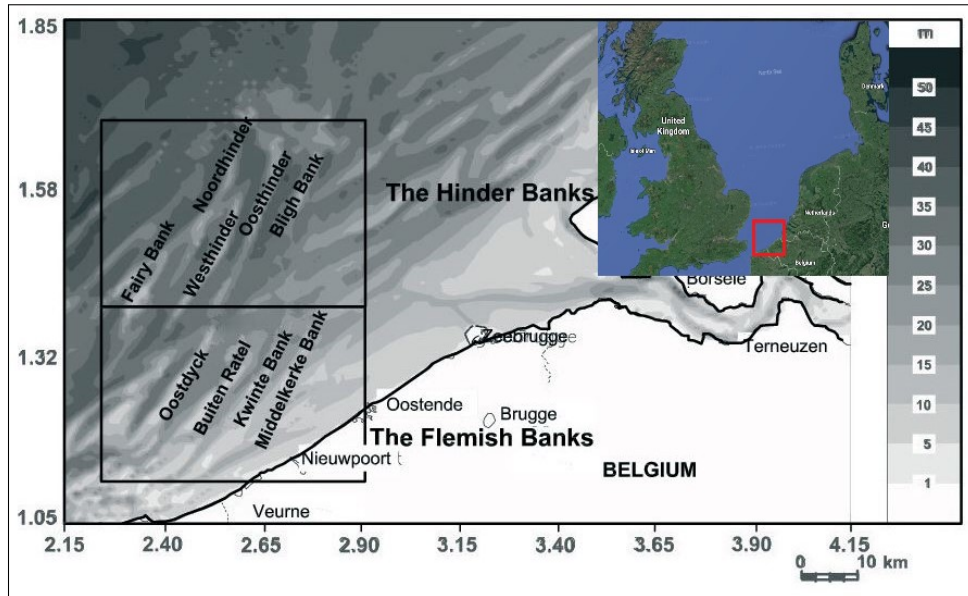


Figure 5: Location and bathymetry of the Belgian coastal area. Adapted from Giardino et al. (2007), where data is provided Flemish Authorities, Agency for Maritime & Coastal Services, Coastal Division. Gridding done by Ghent University, Renard Centre of Marine Geology. The two black rectangles on the map indicate locations of the Flemish banks and the Hinder banks. Map in top right corner displays location Belgian coastal zone, adapted from Google Maps.

The shelf model morphodynamics are solved on a rectilinear, staggered grid. The physical domain has a cross-shore grid resolution Δx ranging between [700, 800] m and an along-shore grid resolution Δy ranging between [700, 900] m. The Delft3D and SWAN domains have Δx ranging between [700, 800] and [700, 1600] m and Δy ranging between [700, \sim 1100] and [700, 2300] m, respectively. The SWAN domain has an equal grid resolution as the Delft3D domain where the two domains overlap and becomes coarser towards its lateral and seaward boundaries.

Since the morphodynamic timescale is much longer (order years) than the hydrodynamic timescale (order days), a morphological acceleration factor f_{MOR} can be used to accelerate the morphological processes (Roelvink, 2006). In this study, a value of $f_{MOR} = 200$ is used, based on a sensitivity analysis (section 4). Using a hydrodynamic time step of $\Delta t = 60$ s, the morphodynamic time step Δt_m becomes 3.33 h. The coupling interval between Delft3D and SWAN is 1 hour. Values of other model parameters of the shelf model are given in table 1.

For the nearshore model, the alongshore grid resolution is equal to the physical domain alongshore resolution Δy ranging between [700, 900] m. Values of other model parameters of the nearshore model are given in table 2.

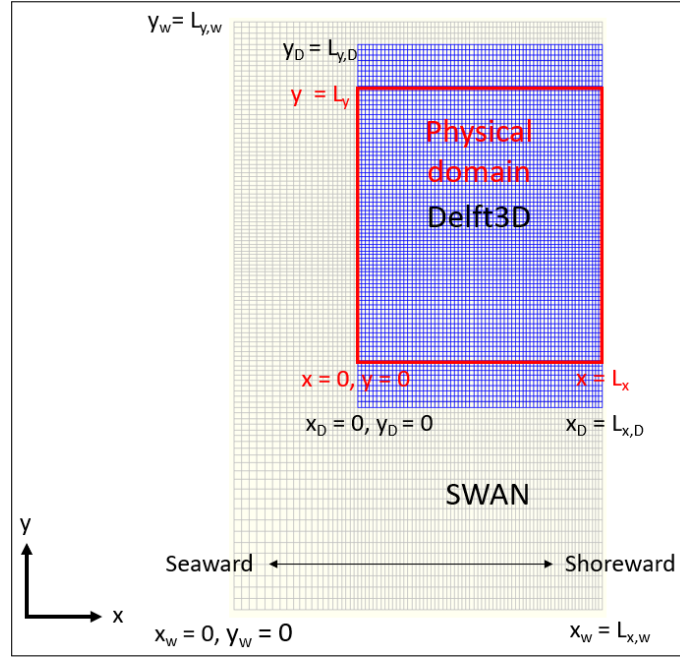


Figure 6: Illustration of grid use. Delft3D (blue grid) and SWAN (grey grid) are the computational domains. Red enlisted area denotes the physical domain.

Table 1

Overview shelf model parameters		
Parameter	Value	Description
Physical domain		
L_x	50 km	Width of domain
L_y	55 km	Length of domain
D_{sea}	38.5 m	Depth at seaward side
$D(L_x)$	5.0 m	Depth at landward side
β	-6.7×10^{-4}	Bottom slope
Flow		
f	$1.43 \times 10^{-4} \text{s}^{-1}$	Coriolis parameter
C	$65 \text{ m}^{1/2} \text{s}^{-1}$	Chezy coefficient
ν	$1 \text{ m}^2 \text{s}^{-1}$	Eddy viscosity
ζ_S, ζ_N	1.8 m , 1.8 m	Amplitude M_2 at south (S), north boundary (N)
ϕ_S, ϕ_N	$0^\circ, 31.5^\circ$	Phase M_2 at south (S), north boundary (N)
ω	$1.405 \times 10^{-4} \text{s}^{-1}$	Angular frequency M_2 tide
Wave		
θ	220°	Wave angle with respect to north (of domain)
H_s	1 m	Significant wave height
T_p	6 s	Peak wave period
$f_s, bins$	$[0.25, 1] \text{ Hz}, 24$	Range wave frequency , number of bins
B_f	$0.035 \text{ m}^2 \text{s}^{-3}$	Bottom friction, JONSWAP
Sediment		
δ	1.66	Relative density of sediment
d_{50}	200 μm	Diameter grain size
α_{BS}	1	Longitudinal bed slope coefficient
α_{BN}	20	Transverse bed slope coefficient
p	0.4	Bed porosity
Numerics		
Δt	60 s	Time step
t_{com}	60 minutes	Communication time Delft3D-Flow and SWAN
α_{mor}	200	Morphological acceleration factor
$\Delta x, \Delta y$	$[700, 800], [700, 900] \text{ m}$	Ranges cross- and alongshore grid cell size for physical domain

Table 2

Overview nearshore model parameters		
Parameter	Value	Description
L_y	55 km	Length of domain
D_c	8 m	Depth of closure
γ	0.88	Depth induced breaking index
k	0.77	Empirical factor (default value)
p	0.4	Porosity
ρ_s	2650 kg/m ³	Sediment density
ρ	1024 kg/m ³	Water density
Δy	[700, 900] m	Range alongshore grid resolution

2.5 Design of experiments

2.5.1 Natural behaviour

To answer research question 1 (i.e. natural (without islands) morphodynamic behaviour of a shelf), the shelf model, where small random bed perturbations h (order cm) are applied on the initial linear sloping bed z_b , will run for 1000 morphological years (spin-up).

2.5.2 Default island case

To answer research question 2 (i.e. quantitative impact artificial islands on shelf morphodynamics, longshore sand transport and coastline change), a sandy (erodible) island is constructed at 10 km distance to the shoreward boundary on the 500 year old spin-up bathymetry (illustrated in figure 7). The island reaches 5 m above MSL and has horizontal dimensions of $l_x \times l_y = 5 \times 10$ km. This experiment will run for 200 morphological years. From here on, this experiment will be referred to as the default island case.

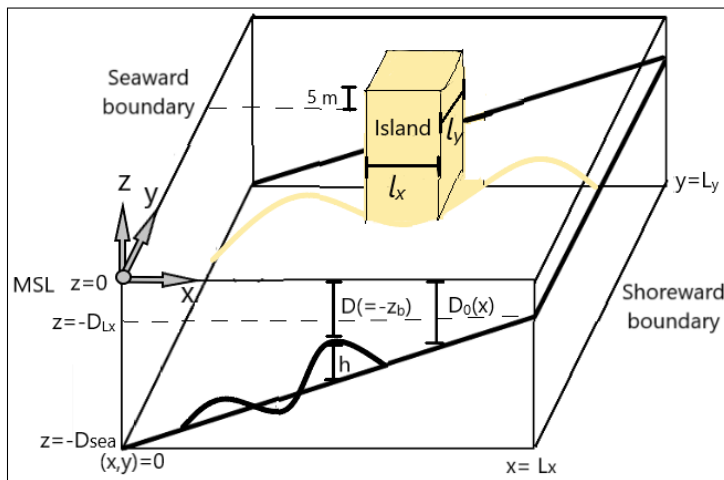


Figure 7: Schematic view of the shelf domain (as in figure 3a) including an (example) island.

2.5.3 Sensitivity experiments: different island configurations

Multiple experiments are carried out in order to find the sensitivity of the model results to the design of sandy (erodible) islands. These experiments will, like the default island case, run for 200 morphological years.

First, the sensitivity of the results to the offshore location of the islands is investigated by conducting experiments where islands are constructed at different distances to the shoreward boundary: 3 km, 15 km, 25 km, 35 km and 45 km .

Second, to quantify the sensitivity of the model results to the geometry of the islands, runs using different island alongshore lengths are conducted ($l_x \times l_y$): 5×5 km, 5×15 km and 5×20 km.

Third, the sensitivity of the results to the number of islands is investigated by conducting experiments using (adjacent in the alongshore direction): two islands and three islands

Last, the effect of the inlet width between alongshore adjacent islands is investigated by conducting experiments using two islands with inlet widths: 5 km and 10 km.

2.6 Methods for analyzing results

The evolution of the intensity of the bedforms in time is measured by their root-mean square height, for a certain domain with area A , defined as

$$h_{rms}(t) = \left(\frac{1}{A} \iint_A h(x, y, t)^2 dx dy \right)^{1/2} \quad (3)$$

in which $h(x, y, t)$ is the bottom perturbation height with respect to the initial bed level $z_b = -D_0(x)$.

The bedforms are further investigated by analyzing the bedform crest and trough volumes V_c and V_t , respectively, defined as

$$V_c(t) = \iint_A h \Theta(h) dx dy \quad \text{and} \quad V_t(t) = \iint_A h(1 - \Theta(h)) dx dy \quad (4)$$

here, $\Theta(h)$ is a Heaviside step function with $\Theta(h) = 0$ for $h \leq 0$ and $\Theta(h) = 1$ for $h > 0$. The V_c measures the excess volume with respect to $z_b = -D_0$, whereas the V_t measures the deficit of volume with respect to $z_b = -D_0$. When an island is included, its volume $V_{island}(t)$ is computed as for V_c , but integrated over the island area.

To investigate the size of the domain area of which its bed has undergone a significant change over time due to the presence of an artificial island, an indicator is introduced that measures the area of morphodynamic influence.

Firstly, the differences between a run with and without an island is given as

$$Z_{b,diff}(x, y, t) = Z_{b,island}(x, y, t) - Z_{b,Noisland}(x, y, t) \quad (5)$$

The area of morphological influence is now defined as

$$AMI(t) = \iint_A \Theta(|Z_{b,diff}| - 0.5) dx dy \quad (6)$$

Thus, an area is considered to be influenced by the island if $Z_{b,diff}$ is larger than 0.5 m.

3 Results

3.1 Natural behaviour

Figure 8 shows coloured contour plots of the depth $-z_b(x, y, t)$ at different times. After 250 years (figure 8b), large-scale elongated bedforms are appearing in the north-western corner of the shelf domain. After 500 years (figure 8c) these bedforms have attained heights up to ~ 20 m, lengths in the order of tens of kilometers and an individual spacing (wavelength) of ~ 7 km. The crests are tilted cyclonically with respect to the principal direction of the tidal current (south to north). These bedform features agree with the characteristics of tidal sand ridges (Dyer and Huntley, 1999). After 1000 years of morphological time (figure 8d), the tidal sand ridges occur everywhere in the shelf domain.

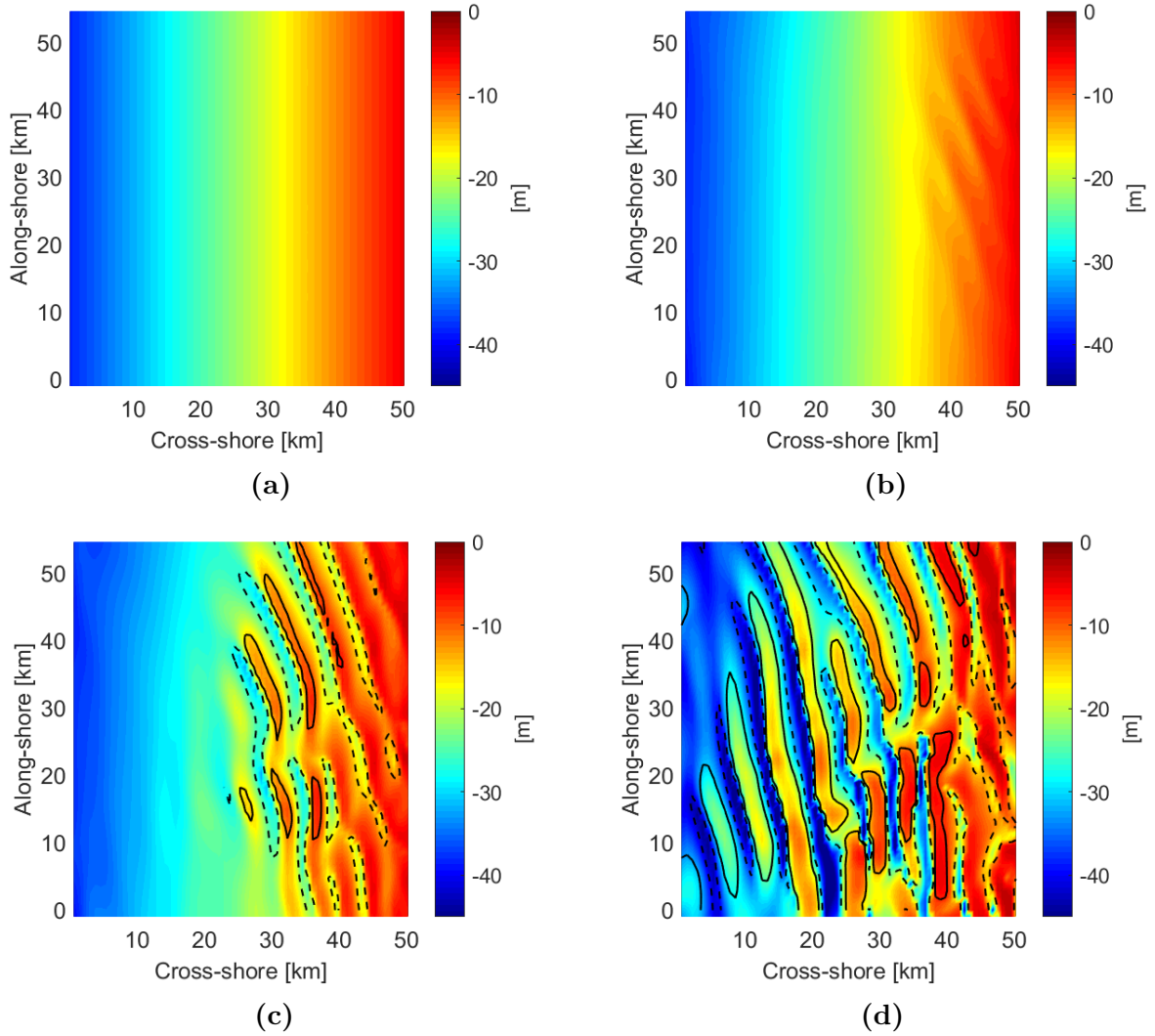


Figure 8: Snapshots of modelled shelf bathymetry at different times during the 1000 year spin-up using a randomly perturbed bed. Black contours (bold, dashed) indicate $h = \pm 5$ m lines. (a) at $t = 0$ y, (b) at $t = 250$ y, (c) at $t = 500$ y and (d) at $t = 1000$ y.

Figure 9a is a contour plot of the bottom perturbation h versus time and cross-shore distance at a cross-shore transect located at $y = 41$ km. It reveals that ridges become noticeable after $300 \sim$ years in the shoreward part ($x > 25$ km) of the domain and they display a small westward migration with a velocity $c_x \sim -1$ km/century. From figure 9b, which shows the bottom perturbation h versus time and along-shore distance at an alongshore transect located at $x = 42$ km, it follows that the ridges migrate southward with velocity $c_y \sim -5$ km/century. Note that for $t > 800$ years this migration is not present anymore.

The time evolution of the root-mean square height h_{rms} of the bedforms in different domains is shown in figure 9c. All curves show initially an rapid increase of h_{rms} , but this increases ceases in the course of time. As the ridges start to form near the coast, h_{rms} in the shoreward part of the domain is at first larger than in the seaward part of the domain, but in the fully developed state, they are approximately the same.

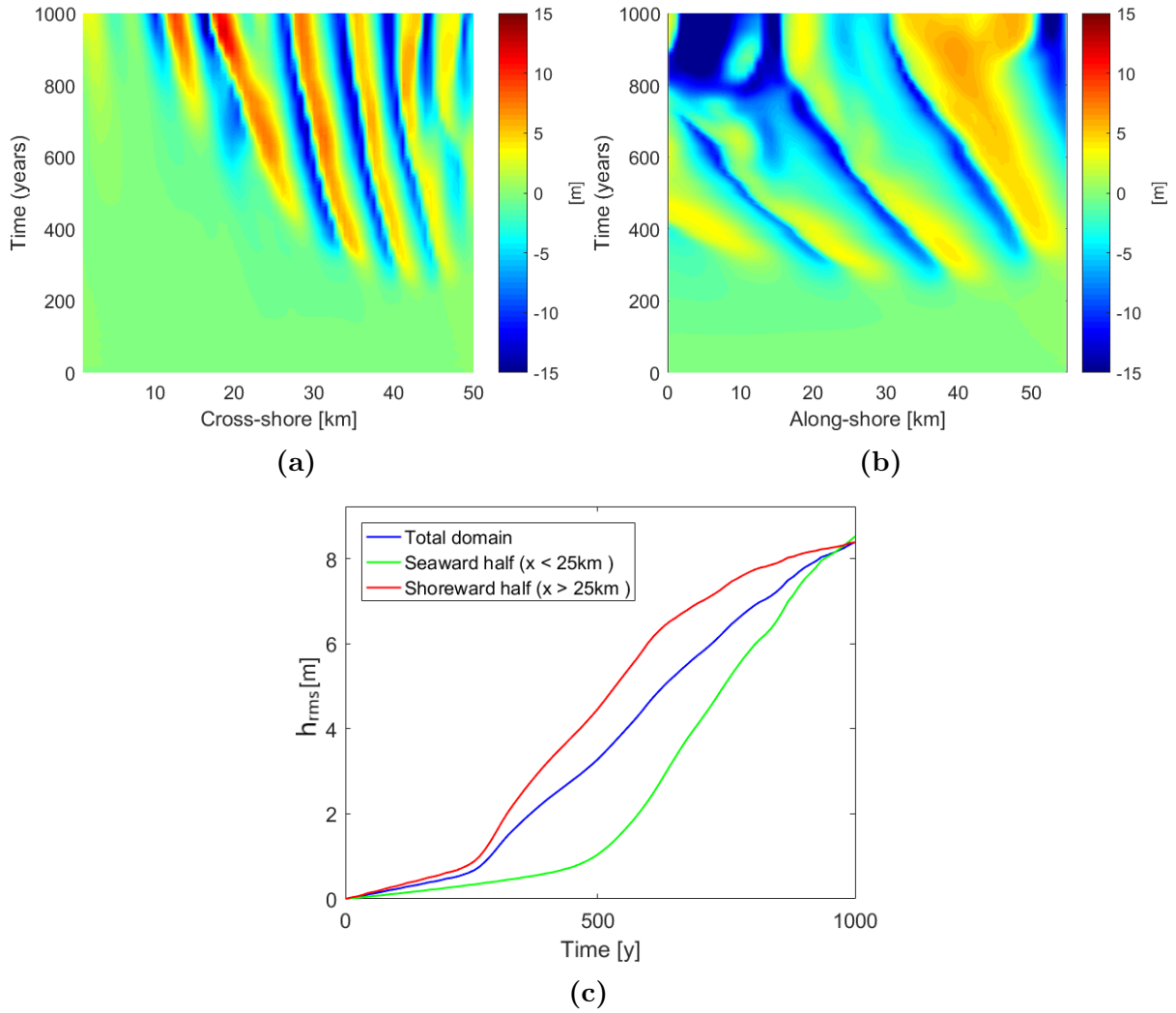


Figure 9: (a) Contour plot of bottom perturbation h (m) along the cross-shore section at $y = 41$ km in the $x - t$ space (x is cross-shore coordinate, t is time). Crests are red and troughs are blue. (b) As in a, but for alongshore section at $x = 42$ km in the $y - t$ space (y is alongshore coordinate, t is time) (c) Time evolution of h_{rms} of bedforms in the entire domain (blue), seaward half (green) and shoreward half (red).

Figure 10a shows the significant wave height distribution (for $x > 20$ km) of a short 5 tidal cycle run on top of the 500 year old spin-up bathymetry. It shows that the significant wave height (H_s) decreases towards the shore and that waves undergo refraction, which is alongshore nonuniform due to the presence of tidal sand ridges. This implies, as can be seen in figure 10b, that the computed longshore sand transport in the surf zone also becomes nonuniform. This figure shows that Q_{vol} has a magnitude in the order of $\sim 4 \times 10^5$ m³/year, which compares well with the longshore sediment transport along the Belgian coast $Q_{vol} = 3.95 \times 10^5$ m³/year found by Verwaest et al. (2011). In the alongshore direction Q_{vol} varies considerably, resulting in erosion ($dQ/dy > 0$) or accretion ($dQ/dy < 0$) rates. These accretion/erosion rates are shown in figure 10c and are in the order of ~ 5 m/y. However, there are some significant peaks in accretion and erosion rates. For instance, around the alongshore position $y = [18, 30]$ km, the accretion and erosion rates have values of ~ 15 m/y and ~ -10 m/y, respectively. These peaks correspond with sharp alongshore gradients in Q_{vol} in figure 10b and hence also with sharp gradients in H_s around $y = [18, 30]$ km at the shoreward boundary (figure 10a). When averaging the accretion and erosion rates over the total alongshore length, a net positive rate of 0.66 m/y is found, implying a net accretion rate for the model domain.

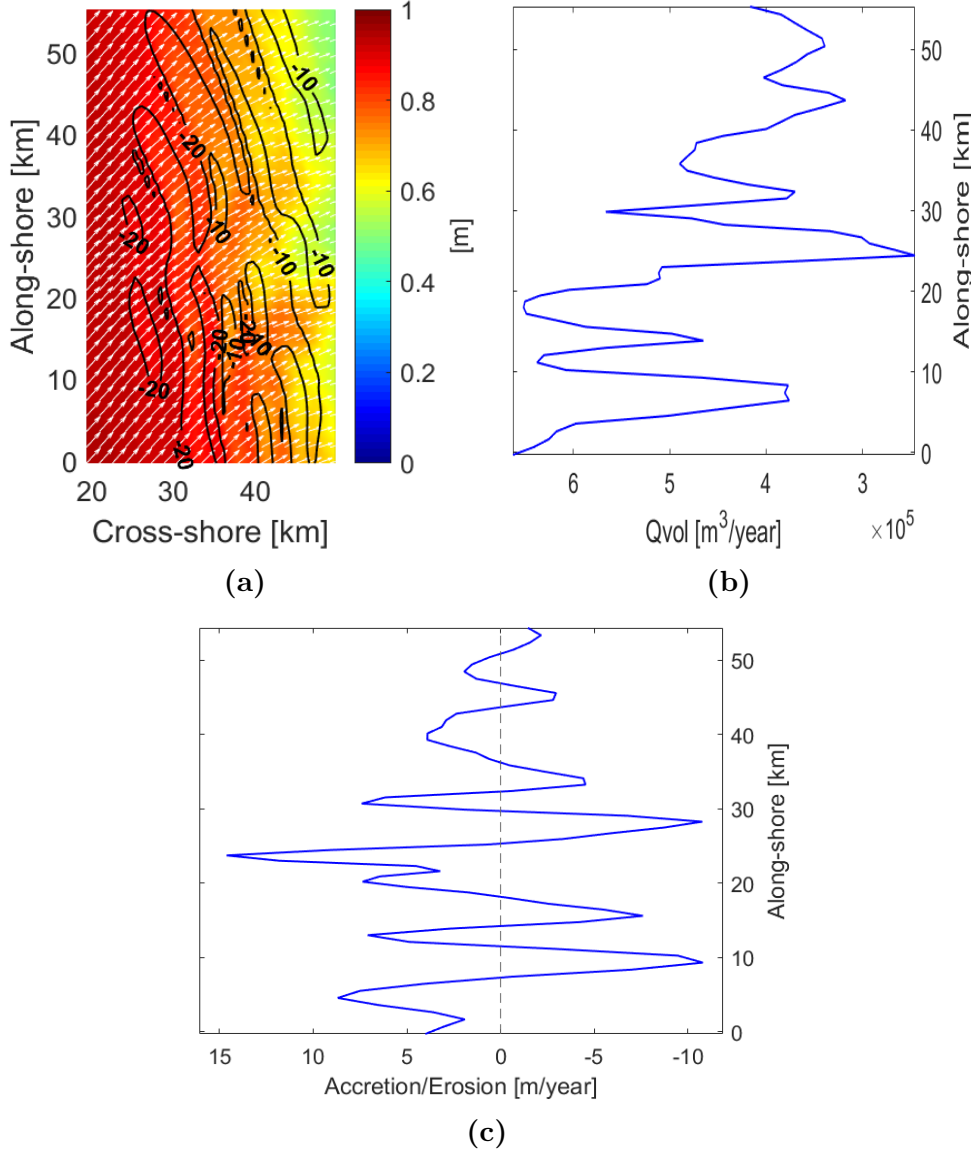


Figure 10: (a) Distribution (for $x > 20$ km) of Significant wave height H_s (colours), after 500 years of spin-up. White vectors indicate wave direction, bed level is indicated by the black contour lines. (b) Longshore sand transport Q_{vol} in the surf zone versus alongshore distance. (c) Coastline accretion and erosion rates versus alongshore distance.

3.2 Presence of islands: default case

Figure 11 shows results for the case that after 500 years of spin-up, the default island (section 2.5.2) is placed 10 km seaward of from the shoreward boundary (at $x = 40$ km, $y = 30$ km). Figure 11a shows the bathymetry 200 years after islands construction, whilst 11b shows the bed level difference with respect to the natural behaviour run after 200 years. Figure 11c shows a colour plot of 200 year bed perturbations h (m) with respect to the 500 year spin-up bed, along the cross-shore section at $y = 41$ km in the $x - t$ space. The white dashed lines display the $h = 5$ m contours for the natural behaviour run. Figure 11d shows the difference in the 200 year bed perturbations h (m) between the default island run and the natural behaviour run, for the same cross-section. By comparing figures 8c, 8d and 11a, clearly, the construction of an island has a large impact on the configurations of the tidal sand ridges. Compared to the natural behaviour run, the ridge crests seaward of the island are less uniformly elongated and have a smaller

anticlockwise angle with respect to the north. In the direct vicinity of the island multiple sand humps have formed. In 200 years time, the island has lost $\sim 40\%$ ($4.5 \times 10^8 \text{ m}^3$) of its sand and rises only partially above the mean sea level. The bed level differences between the natural behaviour and default island run (figure 11b), reveal that in the vicinity of the island, large bed perturbations are organized in alongshore oriented sand ridge like patterns. Comparing bed perturbation evolutions of figures 9a and 11c for $t = [500, 700]$ year and the differences between the black and white crest contour lines ($h = +5 \text{ m}$) for the default island and natural behaviour run (figure 11c), reveal that island construction slightly enhances the seaward migration for ridges in the seaward half of the domain $x < 25 \text{ km}$, whereas ridges are static and deform significantly on the shoreward side $x > 25 \text{ km}$. Figure 11d shows that the bed level differences grow in time and are noticeable ~ 75 years after island construction.

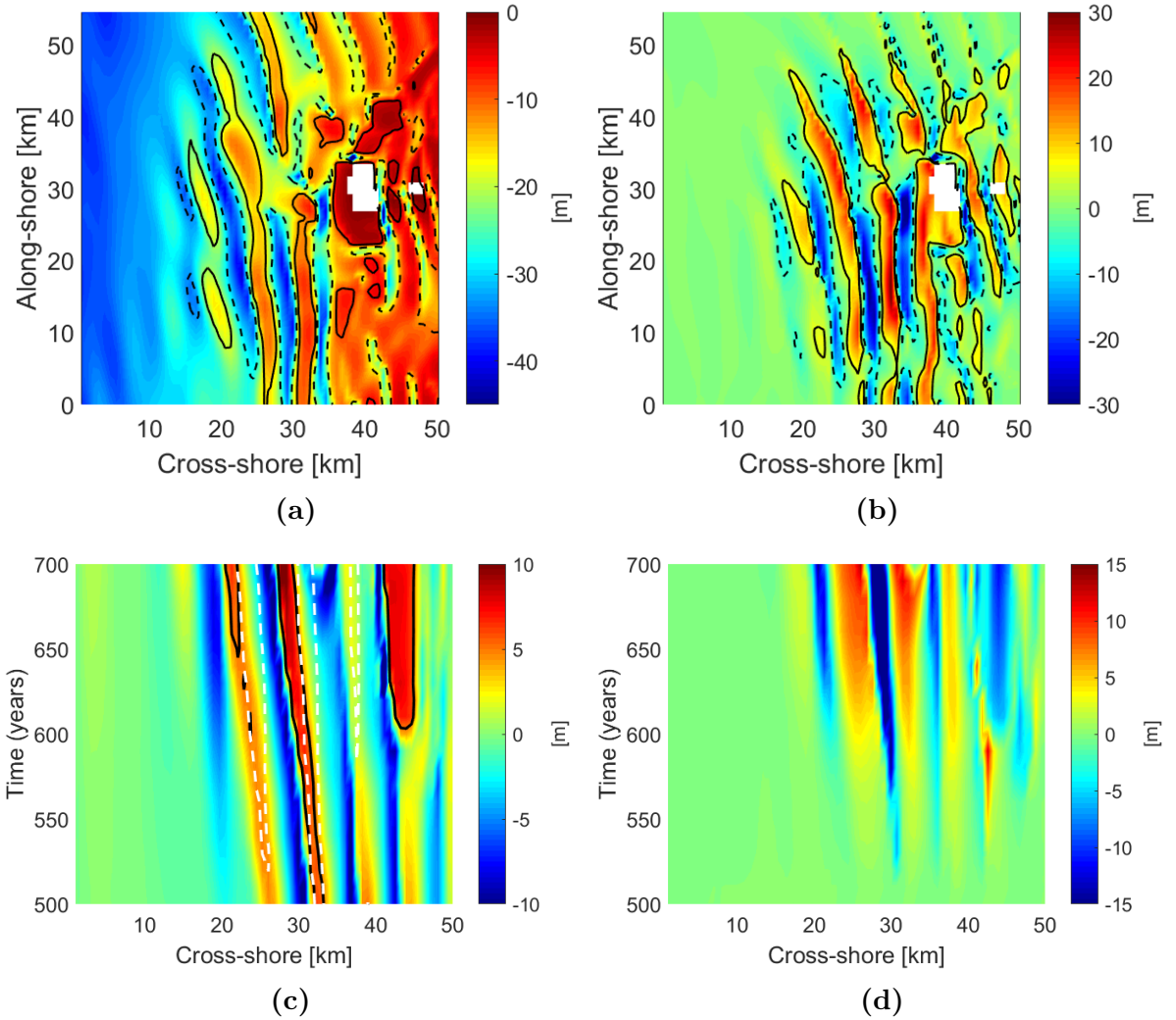


Figure 11: (a) Contour-colour plot showing bed level at time $t = 700$ year, after placement of the default island at $t = 500$ year of the spin-up run. Black contours (bold, dashed) indicate $h = \pm 5 \text{ m}$ lines. (b) As a, but difference in bed level of panel a and spin-up run at $t = 700$ year ($z_{b, island} - z_{b, spin-up}$). (c) Colour plot of 200 year bed perturbations h (m), along the cross-shore section at $y = 41 \text{ km}$ in the $x-t$ space. Crests are red and troughs are blue. (c) Default island run. Black bold (white dashed) contours indicate $h = +5 \text{ m}$ lines for default island (spin-up) run. (d) Same transect as c, but displaying difference Δh ($h_{island} - h_{spin-up}$).

Figure 12a shows time series of crest volume V_c , trough volume V_t and island volume V_{island} for the 200 year period after construction of the island on top of the time series of crest volume V_c , trough volume V_t for the 1000 year natural behaviour run. It appears that in the natural behaviour run, the domain loses sand over time since budget $V_c + V_t < 0$. When an island is constructed at $t = 500$ year, its sand volume decreases over time. This sand is distributed across the domain. The crest volume becomes larger than for the natural behaviour run, whilst the trough volume becomes smaller (infilling with sand). This indicates that the inclusion of an island enhances crest growth, whereas it dampens trough growth. The ongoing decrease in total sand volume of the domain seems to be altered, since the new sand budget including island ($V_c + V_t + V_{island}$) becomes less negative over time.

Figure 12b shows the 200 year evolution of the area of morphological influence (AMI) for the run including an island. It shows that the AMI initially grows rapidly, but flattens out towards the end of the simulation, suggesting that the AMI becomes stable over time.

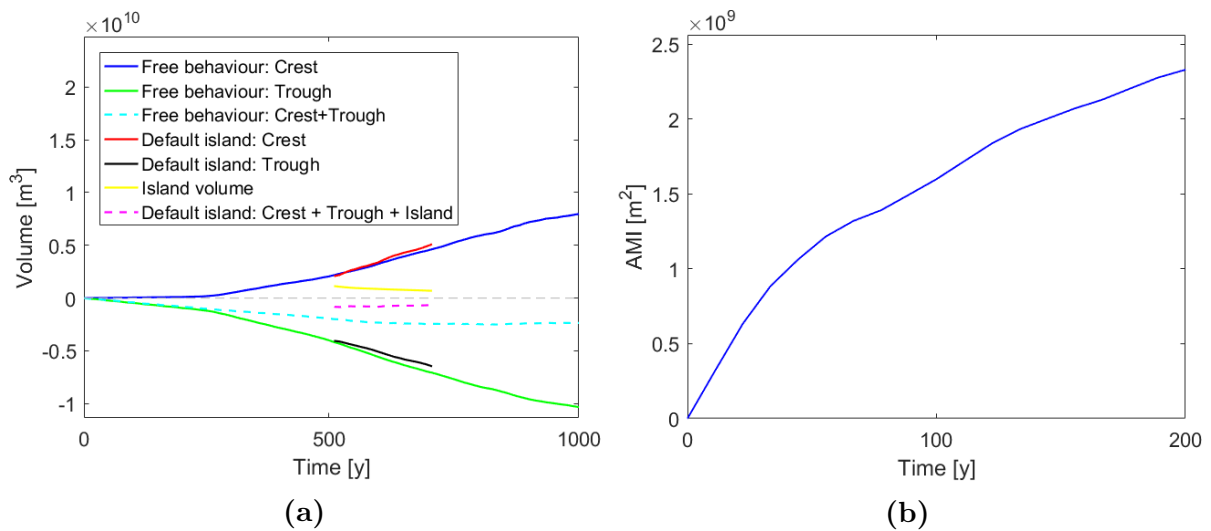


Figure 12: (a) Time series of crest, trough ($V_c(t)$, $V_t(t)$) and total volume for the 1000 year spin-up case and the volumes for the case where at $t = 500$ year an island is constructed (including V_{island}). (b) Time series of the area of morphological influence (AMI) for the 200 years after the island construction (at $t = 500$ year).

The impact of the island on the spatial distribution (for $x > 20$ km) of the Significant wave height (H_s) is shown in figure 13a (as in figure 10a, but now immediately after construction of the island). It shows that shoreward of the island a shadow zone is present, where the H_s is lower than for the natural behaviour case (maximum H_s difference at shoreward boundary is ~ 0.3 m) and waves are strongly refracted. The shadow zone is positioned slightly northward of the island, since the waves propagate in a northeastern direction and stretches alongshore until the northern boundary. Figures 13b and 13c show the Q_{vol} differences and the accretion/erosion rate differences between the case including an island and the natural behaviour run, respectively. They reveal that around the start of the shadow zone $y \sim 25$ km (figure 13a), there is a significant drop in Q_{vol} , resulting in an accretion hotspot (13 m/y) around this position. At the end of the shadow zone $y \sim 40$ km (figure 13a), there is a significant increase in Q_{vol} , resulting in an erosional hotspot (-11 m/y) around this position. When averaging the accretion and erosion rates over the total alongshore length, a net accretion rate of 0.05 m/y is found. This indicates that even though the presence of an island creates large variability in accretion and erosion rates in the model domain, the net rate is not influenced significantly.

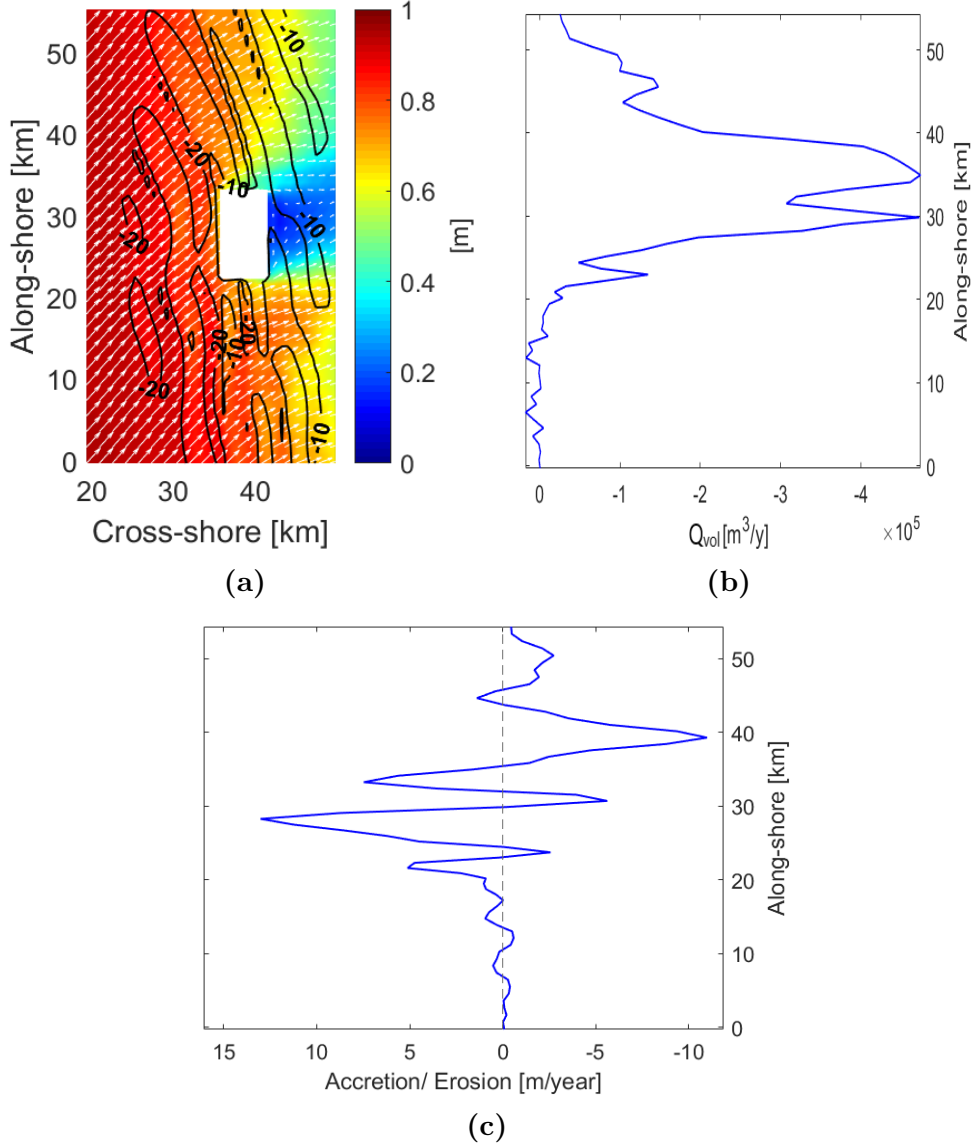


Figure 13: (a) Distribution (for $x > 20$ km) of Significant wave height H_s (colours), after 500 years of spin-up including the default island. White vectors indicate wave direction, bed level is indicated by the black contour lines. (b) Difference in longshore sand transport Q_{vol} between the run including an island and the natural behaviour ($= Q_{vol, island} - Q_{vol, natural\ behaviour}$) versus alongshore distance. (c) Difference in coastal accretion and erosion rates between the run including an island and the natural behaviour run versus alongshore distance.

3.3 Different island configurations

3.3.1 Island distance to coastline

The sensitivity of the morphological impact after 200 years on the shelf and the initial impact on the shoreline change after island construction for islands at different distances to the shoreward boundary are shown in figure 14. Figure 14a shows that for islands near the shoreward boundary (< 10 km), the crest volume growth in 200 years time is slightly larger than the crest volume growth of the natural behaviour case (stars), while trough volume growth is slightly smaller. The smaller trough growth is likely due to the infilling of troughs with sand lost from the island. For the cases where islands are placed further offshore (> 10 km distance), both the crest and trough volume growth is stronger than for the natural behaviour case and increases for offshore island distance. Also, the mass lost

by the island slightly increases for larger island distance. When looking to conservation of total sand in the domain ($\Delta V_c + \Delta V_t + \Delta V_{island} = 0$), it seems that the loss of island sand is not enough to compensate for the difference in crest and trough growth, suggesting that there is extra sand entering into the domain.

Figure 14b shows that, for islands placed further offshore, the area of morphological influence (AMI) after 200 years time, increases, though most increase seems to occur for islands positioned $10 < \text{distance} < 25$ km offshore of the shoreward boundary.

The effect of the island offshore position on the coastline change is shown in figure 14c. Here, the initial mean coastline accretion/erosion rate and its standard deviation are shown for runs with islands at different offshore positions to the shoreward boundary. For small distances to the shoreward boundary (< 10 km), the net rate is almost zero, but grows and attains a maximum around 35 km distance. This is likely due to the northern end of the shadow zone extending beyond the model domain for larger island distances. The standard deviation (denoting the variation in accretion/erosion rates) is in the order of several meters for distances (< 10 km) and decreases significantly for larger distances.

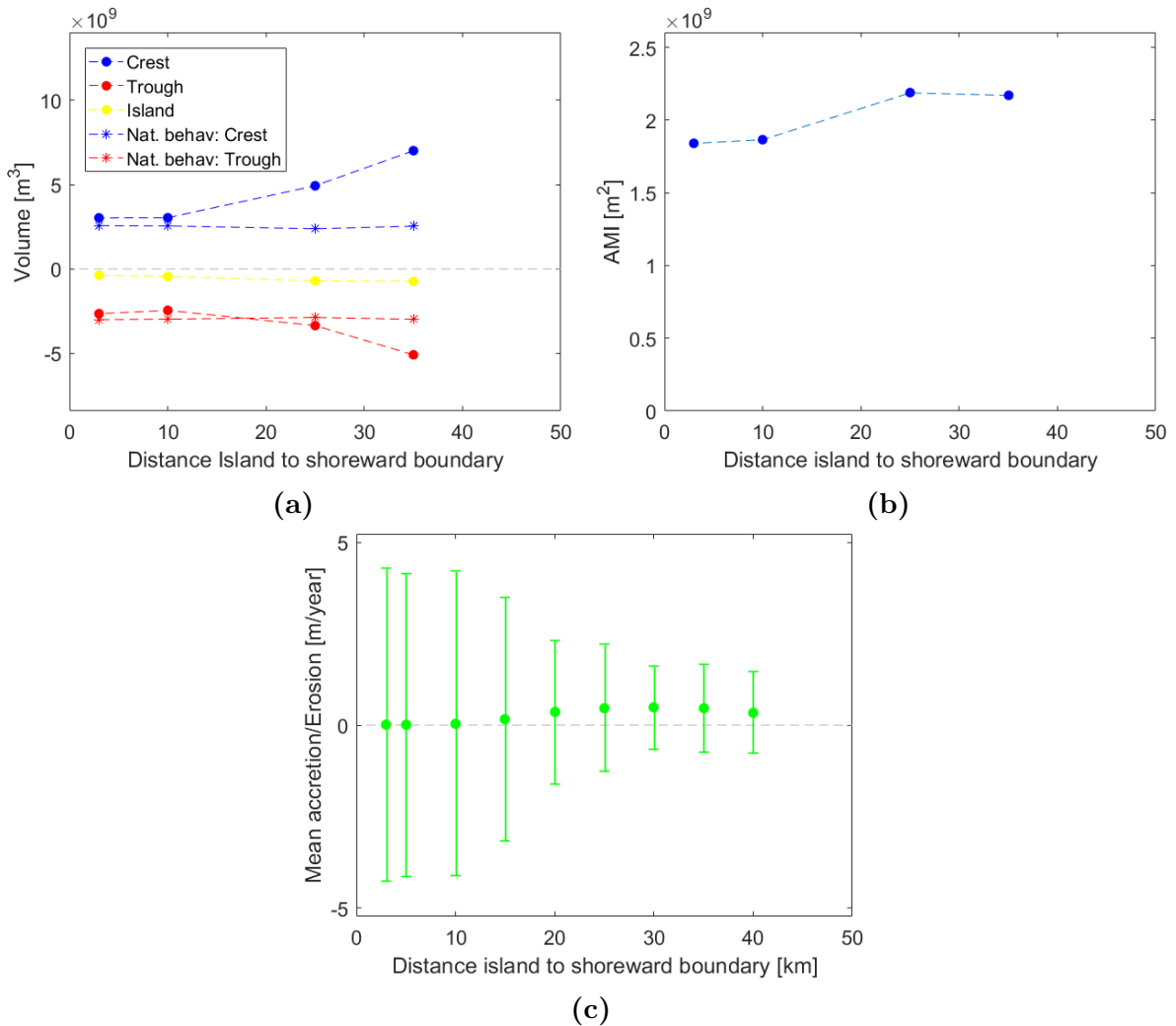


Figure 14: (a) The crest, trough (and island) volume differences after 200 years for the natural behaviour run (stars) and for four runs including an island (dots) at different offshore distances constructed on the 500 year spin-up bed. (b) Area of morphological influence (AMI) after 200 years for four runs with different island distances to the shoreward boundary on 500 year spin-up bed. (c) Initial mean coastal accretion/erosion (=net) rate differences and corresponding standard deviation with respect to the natural behaviour run, for six runs with islands at different distances to the shoreward boundary (constructed on 500 year spin-up bed).

3.3.2 Island size (varying alongshore length)

The sensitivity of the morphological impact after 200 years on the shelf and the initial impact on the shoreline change after island construction for islands having different alongshore lengths are shown in figure 15. Figure 15a shows that for a larger island size, the crest growth with respect to the natural behaviour case becomes larger and this difference increases for an increasing island size. The trough volume growth with respect to the natural behaviour case is for all island sizes smaller (due to sand infilling) and decreases only slightly for larger islands. This implies that mainly the crest growth benefits from an increasing island size, whereas the decrease in trough volume growth does not significantly depend on the island size.

Figure 15b shows that the *AMI* normalized by the island area, on the coastal shelf decreases for an increasing alongshore island length. This indicates that a small island alters the shelf bed in a larger area (per m^2 island area) than a longer elongated island does.

The effect of the alongshore island length on the coastline change is shown in figure 15c. This figure shows that for an increasing alongshore island size, the mean (net) rate remains for all cases approximately zero. The standard deviation however increases. This suggests that when an island becomes longer, a stronger shadow zone is created, resulting in intenser accretion and erosion hot-spots at the begin and end of the shadow zone.

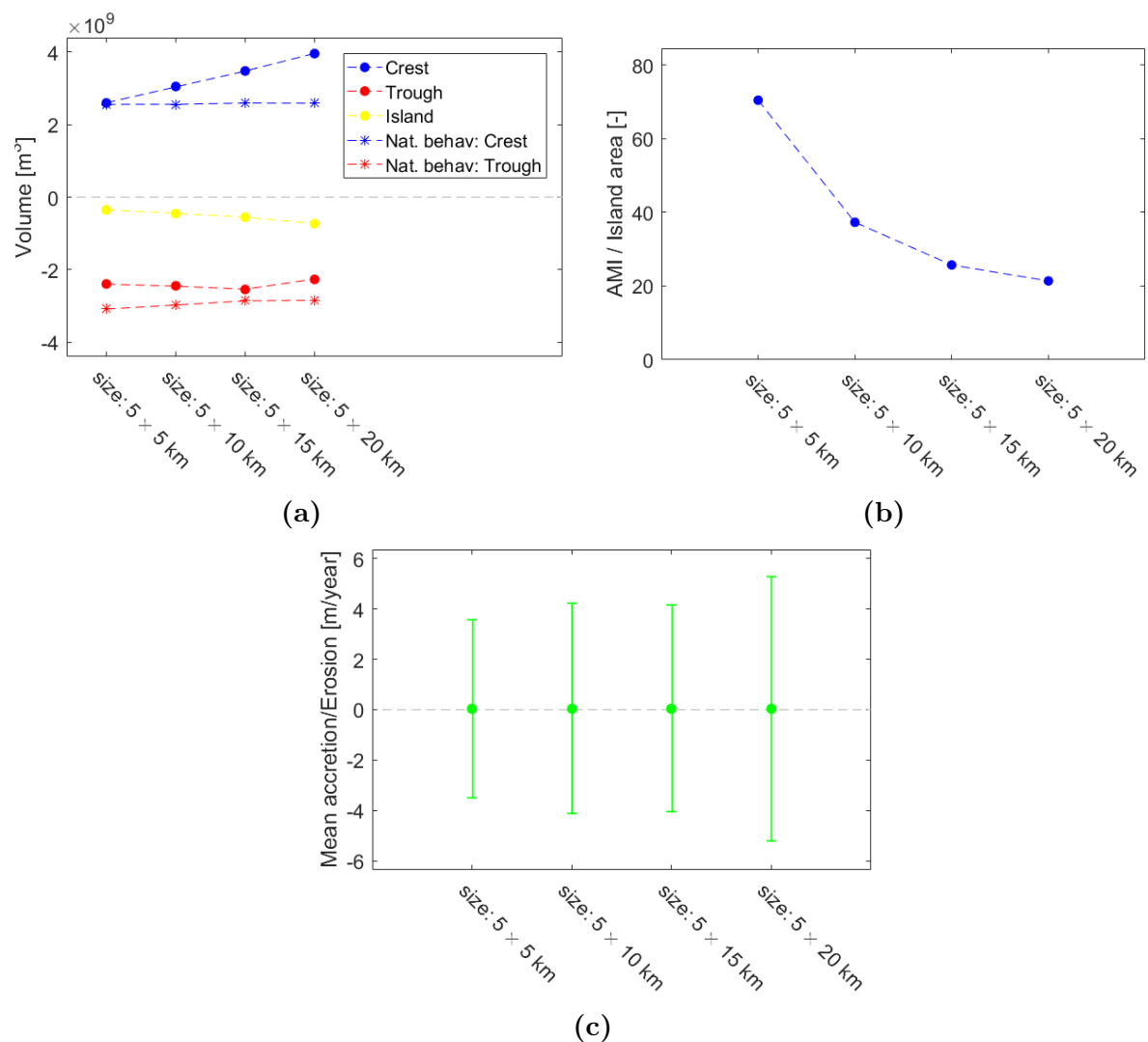


Figure 15: (a, b, c) As in figure 14, but now for four cases with islands having different alongshore lengths. (b) Note that the *AMI* here is normalized by the island area.

3.3.3 Multiple islands

Figure 16a, shows when two islands are constructed instead of one, the difference in crest volume growth with respect to the natural behaviour case increases, whereas the trough volume growth difference with respect to the natural behaviour case decreases. When including three islands, mainly the crest growth difference increases, implying that more island sand is distributed on top of the crests than for the cases when one or two islands are constructed.

Figure 16b shows that the *AMI* per m^2 island area, is largest in case of one island and becomes smaller for increasing the number of constructed islands from two to three.

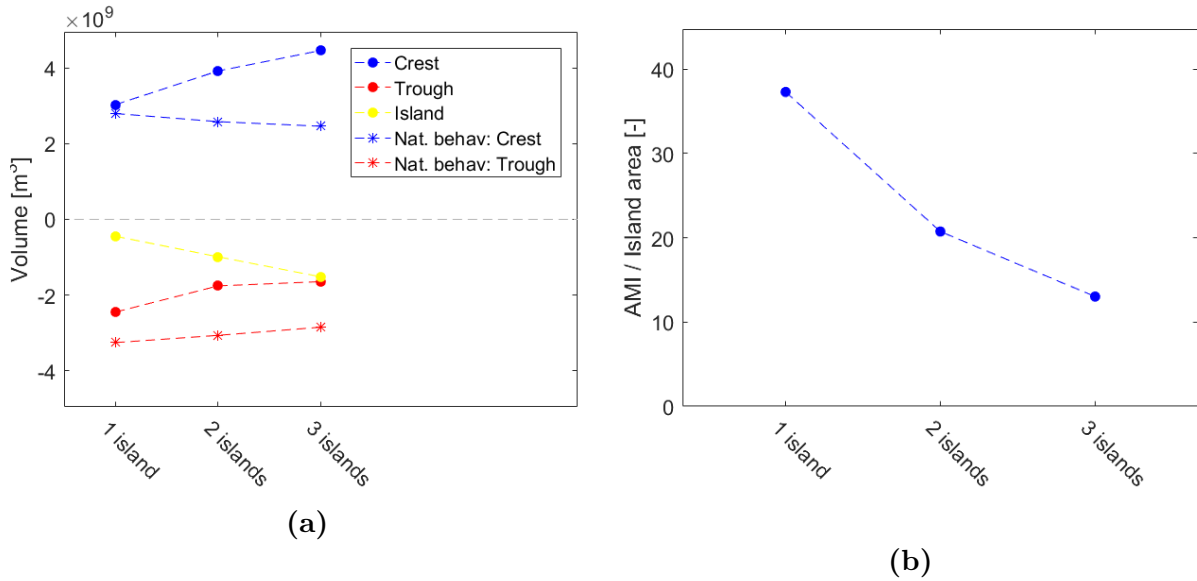


Figure 16: (a, b) As in figures 14a and 14b, but now for varying the number of constructed islands instead of varying the island position towards the shoreward boundary. (b) Note that the AMI here is normalized by the total area occupied by island(s).

3.3.4 Variable inlet width

For the sensitivity analysis to investigate the effect of multiple islands on the shoreline change, the alongshore domain length is too small. Therefore only the effect of the inlet size between two island is investigated and shown in figure 17. It shows that when an island of size (size: $5 \times 20 \text{ km}$) is divided in to two smaller islands (sizes: $5 \times 10 \text{ km}$) with an inlet of 5 km in between, the mean (net) rate stays approximately zero but the standard deviation increases. The enlargement of the inlet size (10 km) does not have a significant impact on the mean rate (remaining \sim zero). The standard deviation decreases slightly for an increasing inlet width $> 5 \text{ km}$.

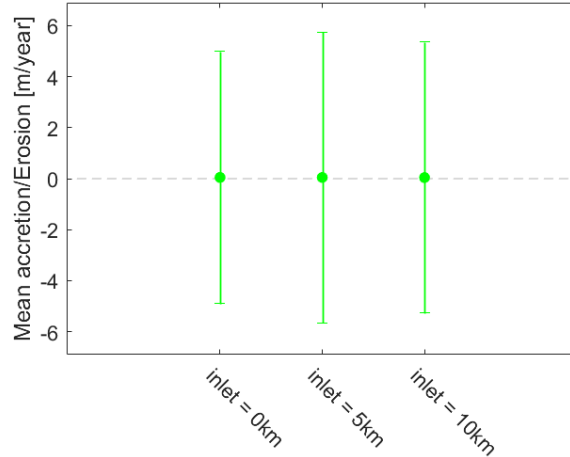


Figure 17: Initial mean coastal accretion/erosion (=net) rate differences and corresponding standard deviation with respect to the natural behaviour run, for three runs where an island (size: 5×20 km) is divided into two smaller islands (size: 5×10 km) with two different inlet sizes (constructed on 500 year spin-up bed).

4 Discussion

4.1 Physical analysis

4.1.1 Natural behaviour: formation tidal sand ridges

This study shows for the first time, using a numerical morphodynamic model including both suspended and bedload transport, a sloping bed and wave effects, that mature tidal sand ridges form on the shelf. The work thus extends earlier studies by [Huthnance \(1982a\)](#), [Roos et al. \(2004\)](#), [Yuan et al. \(2017\)](#) and [van Veelen et al. \(2018\)](#). Note that [Calvete et al. \(2001\)](#) also found tidal sand ridges on a shelf with a sloping bottom, but they considered only the initial formation of the ridges and they did not account for waves and suspended load transport.

Studies by [Zimmerman \(1981\)](#) and [Huthnance \(1982a\)](#) explain the growth of these bedforms in terms of residual currents that are generated by tide-topography interaction. According to their theory, the preferred ridges have crests that are rotated cyclonically with respect to the direction of the principal tidal current. Furthermore, anticyclonic residual current cells occur around the ridges. The preferred crest orientation is due to the Coriolis force. In that case the residual currents are maximum and that is important for ridge growth. This is because during the ebb and flood, the total flow (tidal + residual) velocity is larger on the upstream side of the ridge than on its downstream side. As sand transport increases faster than linear with increasing magnitude of the flow velocity, net accumulation of sand occurs in the ridge area. In case the principal current is asymmetric, the ridge will migrate in the direction of its peak value ([Walgreen et al., 2002](#)). To verify whether this theory also explains the sand ridges obtained in this study, figure 18 shows a map of a modelled tidal sand ridge with the (tidally averaged) residual currents vectors displayed. Clearly, the residual velocity vectors show a clockwise (i.e. anticyclonic on the Northern hemisphere) pattern around the sand ridge crest. Due to the difference in residual current magnitude at the seaward and shoreward side of the ridge, the sand ridge migrates in the seaward direction.

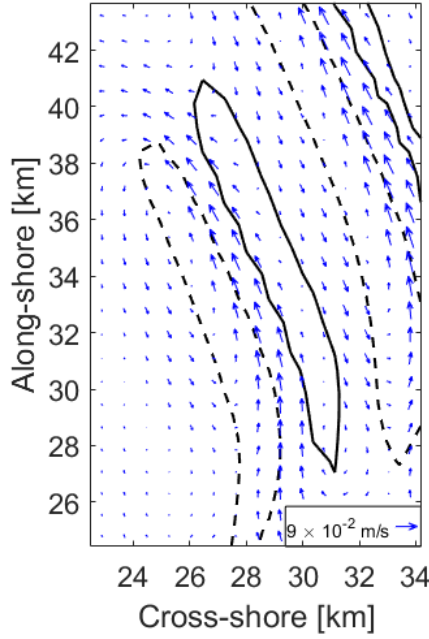


Figure 18: Map of a modelled tidal sand ridge, after 500s of spin-up, showing the residual currents vectors (tidally averaged). Black contours (bold, dashed) indicate $h = \pm 5$ m lines.

4.1.2 Default island: residual currents and sand transport on shelf

Figure 19 shows, that when an island is placed at a shelf with a linear sloping bottom, residual currents are generated around the island. These are largest (~ 0.2 m/s) near the north-west and south-east tip of the island and display clockwise circulations cells. These results qualitatively agree with those of [Roos et al. \(2008\)](#), who showed that in the case of constructing a sand pit on a shelf with a constant depth, similar residual flow cells around the pit are present. They found that the residual flow is generated due to bottom friction (inversely proportional to water depth) and enhanced by Coriolis effects.

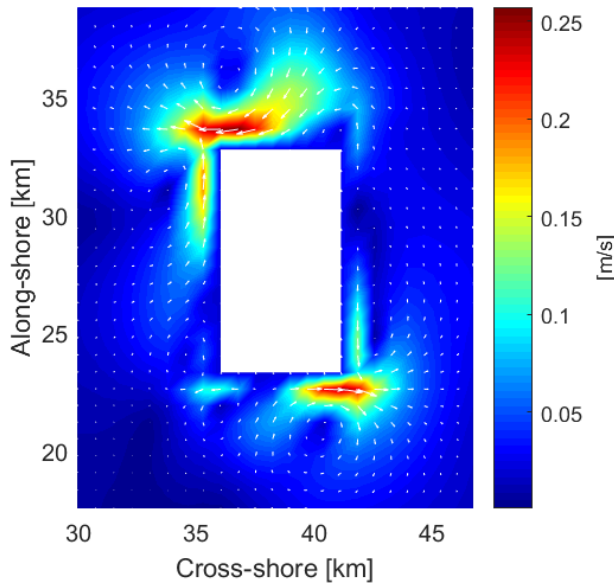


Figure 19: Map showing tidally averaged residual velocities (color scale and white vectors) that are generated by an island placed on a shelf with a sloping bed.

In section 3, the default island was placed upon a shelf that is characterized by mature sand ridges. Again (figure 20), residual currents are present at the north-western island corner

(~ 0.25 m/s), which are significantly larger than those at the south-east island corner (~ 0.15 m/s). Figure 20b shows (for the same run), a strong divergence (erosion) spot in the vicinity of the north-western island corner with an adjacent convergence (accumulation) spot. The magnitude of this erosion and accumulation of sand (10^{-7}) is two orders of magnitude larger than the erosion and accumulation for a run without an island (10^{-9}). This implies that the island initially loses much of its sand locally around one island corner, which accumulates directly next to it. These findings are again consistent with Roos et al. (2008), where they found that the pit deepens and deforms around these pit corners into the direction governed by Coriolis effects.

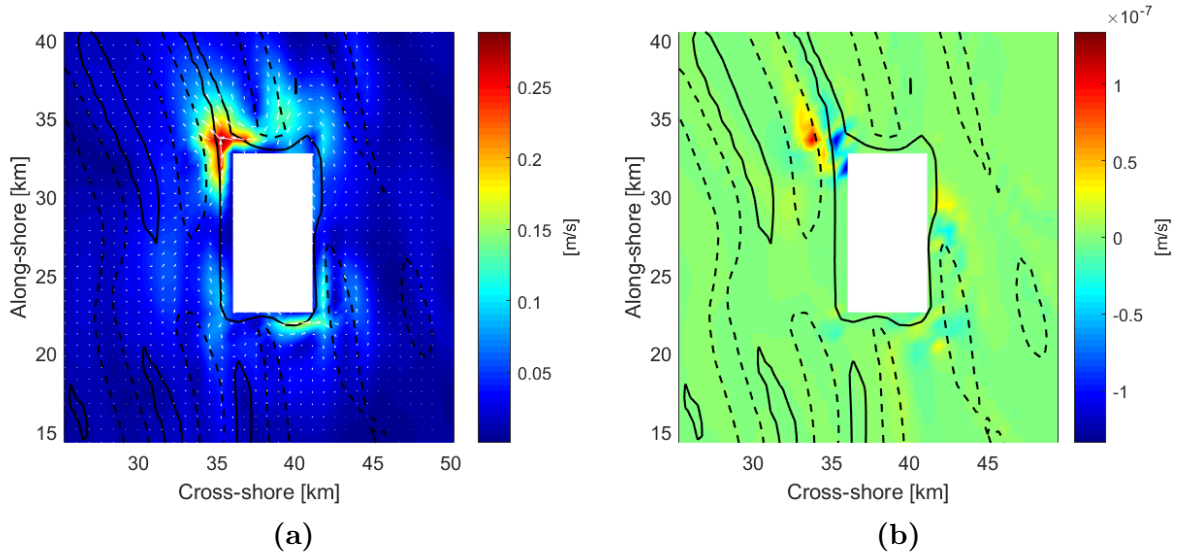


Figure 20: Maps (zoomed in around island) showing differences in tidally averaged quantities between run with island and natural behaviour run. Black contours (bold and dashed), are $h = \pm 5$ m lines. (a) Residual current (color scale and white vectors). (b) Convergence of total transport by volume (color scale).

4.1.3 Shoreline change: effect of multiple wave conditions

In section 3.1 it was pointed out that there are large coastal accretion and erosion rates for the natural behaviour case. This results in too large yearly shoreline accretion and erosion rates (figure 10c). Therefore, a sensitivity experiment using four dominant wave conditions (table 3) has been conducted for one case without island (figure 21) in order to analyse its effect on the shoreline change rates. It is found that by using multiple wave conditions, the coastline variance decreases.

The large shoreline variance (e.g. distinct peaks in figure 13c) caused by a shadow zone which is created when an island is included, might also become lower when averaging over multiple wave conditions, as the position of the shadow zone and resulting gradients in longshore sand transport depend on the wave angle and magnitude.

The usage and effect of including multiple wave conditions requires further study.

Table 3

Wave conditions				
	H_s	$\theta(^{\circ})$	T_p (s)	Probability
Condition 1	0.67	181	4.86	0.0562
Condition 2	0.92	220	5.7	0.3666
Condition 3	0.80	276	6.75	0.3440
Condition 4	0.75	316	6.48	0.2332

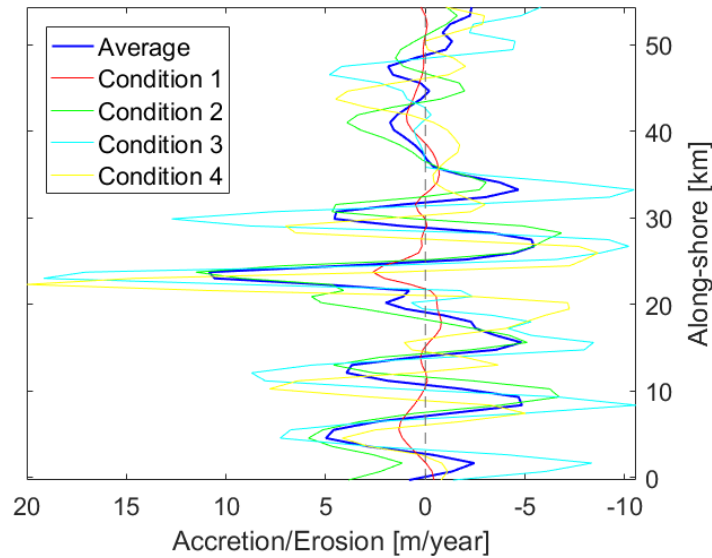


Figure 21: Alongshore coastal accretion and erosion rates using four different wave conditions for the natural behaviour case (500 year bathymetry state, averaged over five tidal cycles). The lines indicate the individual runs of the four wave conditions and their average.

4.1.4 Sand volume budget of domain

In section 3.2, it was stated that the domain loses sand volume over time, whereas when an island is included, it tends to gain sand volume. In section 3.3.1 it was found that this effect increases when islands are placed at a larger distances to the shoreward boundary. A possible explanation for this offset could be that sand is lost or gained by transport through the domain boundaries. So far, the sand fluxes over the domain boundaries have not been investigated and are therefore an important topic for further research.

4.2 Sensitivity analysis

4.2.1 Numerical parameters

A sensitivity analysis to the time step (Δt) up-scaling has been carried out for a spin-up run using $\Delta t = 30$ s and $\Delta t = 60$ s. Since no significant differences in the results were found, a time step of $\Delta t = 60$ s for the subsequent experiments has been used.

Another sensitivity analysis regarding the Morfac up-scaling showed no differences in the results when using Morfac's 50, 100 and 200. Therefore, a Morfac of 200 was chosen.

4.2.2 Sand transport equation

A sensitivity analysis, carried out to investigate the effect of the chosen sand transport equation on the model results, showed that using the formulation from [Van Rijn \(1993\)](#) and the Soulsby-Van Rijn formulation ([Soulsby, 1997](#)), that in both cases tidal sand ridges develop on the shelf having equal properties. This reveals that the model results do not depend on the use of one specific transport equation.

4.3 Physical limitations

Using the shelf model in a 2DH mode, three-dimensional processes (e.g. undertow) can not be taken into account. Hereby, the onshore sand transport due to wave asymmetry has not been taken into account.

For the tidal forcing a single M_2 has been used, whereas its overtides and other tidal constituents are also present in the Belgian coastal area. However, other tidal constituents (such as S_2) have only a small contribution to the long-term mean sand transport (Van de Kreeke and Robaczewska, 1993).

A further limitation, concerns the fact that the nearshore zone model does not incorporate the interaction between coastline change and nearshore zone and shelf bathymetry, only the instant shoreline change rates can be determined. Therefore in further studies, a 2D nearshore zone evolution model (e.g. Arriage et al. (2017)) is needed that accounts for this coupling (feedback), in order to evaluate the long-term shoreline evolution.

Also, the effects of sea level rise (SLR) have not been taken into account. Uehara et al. (2006) showed that for the Holocene period, SLR can alter the strength and orientation of the tidal currents significantly. SLR can also alter the sea bed interaction with waves, as the wave-induced bed shear stress is sensitive to changes in total water depth (Neill et al., 2009). As these changes occur on the same time scale as the evolution of tidal sand ridges, ridge growth can be altered (Yuan and de Swart, 2017).

5 Conclusions

The main findings of this study are the following. First, the formation of free mature tidal sand ridges is simulated with a numerical morphodynamic model on a shelf with a sloping bottom that accounts for tides, waves, bedload transport and suspended load transport. Their patterns, growth and migration can be explained with the classical theory of Huthnance (1982a). These ridges have a profound impact on the dynamics of the surf zone, by creating peaks in the accretion and erosion of the coastline with values in the order of several meters per year.

Second, when implementing an island on the shelf, it is found that there is initially strong erosion of sand at the north-west island tip. Eroded island sand is distributed across the domain and is used to increase the volume of the crests and to fill in the troughs of the ridges. The migration and characteristics of the tidal sand ridges are mainly altered in the vicinity of the island, whereas the shelf further offshore undergoes less significant bed change. After the construction of an island, a shadow zone is created shoreward of the island, where the significant wave height is dampened and waves display refraction. This gives rise to accretion of the coast behind the island and erosion further downstream, however the net change of the coastline remains almost unchanged.

By studying different island configurations, it is found that the area in which the bed level is influenced by an island increases when an island is placed further offshore. Normalized by the island area, the area in which the bed level is influenced by an island, decreases when an island has a longer alongshore length or for an increasing number of adjacent islands. The crest and trough volumes both grow for an increasing island distance to the coast, while for an increasing island length only the crest volume grows. For an increasing number of alongshore adjacent islands, the crest volume grows, whereas the trough volume growth becomes smaller.

The variance in coastline accretion/erosion rates in the model domain decreases when islands are placed further offshore, though the small net accretion rate increases. For an increasing island size, the variance in coastline accretion/erosion rate increases, but the net remains almost zero. In the case of two islands, separated by an inlet, variance in accretion/erosion rates increase for wider inlets, but the increase is minimum once the width is larger than 5 km. The net rate remains very small for all cases.

References

- J. Arriage, J. Rutten, F. Ribas, A. Falqués, and B.G. Ruessink. Modeling the long-term diffusion and feeding capability of meganourishment. *Coastal Engineering*, 121:1–13, 2017.
- N. Booij, L.H. Holthuijsen, and L.C. Ris. The SWAN wave model for shallow water. *25th International Conference on Coastal Engineering*, 1996. doi: 10.1061/9780784402429.053.
- D. Calvete, M. Walgreen, H.E. De Swart, and A. Falqués. A model for tidal sand ridges on the shelf: Effect of tidal and steady currents. *Journal of Geophysical Research*, 106(C5): 9311–9325, 2001. doi: 10.1029/2001JC900001.
- C.J. Crossland, H.H. Kremer, H. Lindeboom, J.I. Marshall Crossland, and M.D.A. (Eds.) Le Tissier. *Coastal Fluxes in the Anthropocene: The Land-Ocean Interactions in the Coastal Zone Project of the International Geosphere-Biosphere Programme*. Springer, 2005.
- R.K. Dyer and D.A. Huntley. The origin, classification and modelling of sand banks and ridges. *Continental shelf research*, 19:1285–1330, 1999. doi: 10.1016/S0278-4343(99)00028-X.
- A. Falqués and D. Calvete. Large-scale dynamics of sandy coastlines: Diffusivity and instability. *Journal of Geophysical Research*, 110, 2005. doi: 10.1029/2004JC002587.
- A. Giardino, D. Van den Eynde, and J. Monbaliu. Wave effects on the morphodynamic evolution of an offshore sand bank. *Journal of Coastal Research*, 51:127–140, 2007. doi: 10.2112/SI51-012.1.
- H. Hanson, A. Brampton, M. Capobianco, H.H. Dette, L. Hamn, C. Laustrup, A. Lechuga, and R. Spanhoff. Beach nourishment projects, practices, and objectives a European overview. *Coastal Engineering*, 47:88–111, 2002.
- C. Hilton and R.J. Nicholls. Spatial and temporal behaviour of depth of closure along the Holland coast. *26th International Conference on Coastal Engineering*, pages 2913–2925, 1998. doi: 10.1061/9780784404119.221.
- J.M. Huthnance. On one mechanism forming linear sand banks. *Esutarine, Coastal and Shelf Science*, 14:79–99, 1982a.
- IPCC. *Climate Change 2014: Synthesis Report. Contribution of Working Groups I, II and III to the Fifth Assessment Report of the Intergovernmental Panel on Climate Change [Core Writing Team, R.K. Pachauri and L.A. Meyer (eds.)]*. IPCC, Geneva, Switzerland, 2014.
- J.M. Keenan and C. Weisz. *Blue Dunes Climate Change by Design*. Columbia Books on Architecture and the City, Columbia University Press 61 West 62 Street New York, NY 10023, 2017.
- P.D. Komar. *Beach processes and sedimentation second edition*. Prentice Hall, Upper Saddle River, New Jersey 07458, 1998.
- G.R. Lesser, J.A. Roelvink, J.A.T.M. Kestera, and G.S. Stelling. Development and validation of a three-dimensional morphological model. *Coastal Engineering*, 51:883–915, 2004. doi: 10.1016/j.coastaleng.2004.07.014.
- A.P. Luijendijk, R. Ranasinghe, M.A. de Schipper, B.A. Huisman, C.M. Swinkels, D.R. Walstra, and Stive M.J.F. The initial morphological response of the sand engine: A process-based modelling study. *Coastal Engineering*, 119:1–14, 2017. doi: 10.1016/j.coastaleng.2016.09.005.

- S.P. Neill, J.D. Scourse, G.R. Bigg, and K. Uehara. Changes in wave climate over the north-west European shelf seas during the last 12,000 years. *Journal of Geophysical Research*, 114 (C06015), 2009. doi: 10.1029/2009JC005288.
- A. Nnafie, H.E. de Swart, D. Calvete, and R. Garnier. Modeling the response of shoreface-connected sand ridges to sand extraction on an inner shelf. *Ocean Dynamics*, 64:723–740, 2014. doi: 10.1007/s10236-014-0714-9.
- F. Ribas, A. Falqués, H.E. de Swart, N. Dodd, R. Garnier, and D. Calvete. Understanding coastal morphodynamic patterns from depth-averaged sediment concentration. *Reviews of Geophysics*, 53(13):362–410, 2015. doi: 10.1002/2014RG000457.
- D. Roelvink and D. Walstra. Keeping it simple by using complex models. *Advances in Hydro-Science and -Engineering*, 6, 2004.
- J.A. Roelvink. Coastal morphodynamic evolution techniques. *Coastal Engineering*, 53:277–287, 2006. doi: 10.1016/j.coastaleng.2005.10.015.
- P.C. Roos, S.J.M.H. Hulscher, M.A.F. Knaapen, and R.M.J. Van Damme. The cross-sectional shape of tidal sandbanks: Modeling and observations. *Journal of Geophysical research*, 109, 2004. doi: 10.1029/2003JF000070.
- P.C. Roos, S.J.M.H. Hulscher, and H.J. de Vriend. Modelling the morphodynamic impact of offshore sandpit geometries. *Coastal Engineering*, 55, 2008. doi: 10.1016/j.coastaleng.2008.02.019.
- USACE Shore Protection Manual. *Shore Protection Manual*. Waterways Experiment Station, Vicksburg, USA, 1984.
- R. Soulsby. *Dynamics of marine sands: A manual for practical applications*. Telford, London, 1997.
- K. Uehara, J.D. Scourse, K.J. Horsburgh, and A.P. Purcell. Tidal evolution of the northwest European shelf seas from the last glacial maximum to the present. *Journal of Geophysical Research*, 111(C09025), 2006. doi: 10.1029/2006JC003531.
- J. Van de Kreeke and K. Robaczewska. Tide-induced residual transport of coarse sediment application to the Ems estuary. *Netherlands Journal of Sea Research*, 31(3):209–220, 1993. doi: 10.1016/0077-7579(93)90022-K.
- L.C. Van Rijn. *Principles of Sediment Transport in Rivers, Estuaries and Coastal Seas*. Aqua Publications, Amsterdam, 1993.
- E. Van Slobbe, H.J. de Vriend, S. Aarninkhof, K. Lulofs, M. de Vries, and P. Dircke. Building with nature: in search of resilient storm surge protection strategies. *Natural Hazards*, 66(13): 1461–1480, 2013. doi: 10.1007/s11069-012-0342-y.
- T.J. van Veelen, P.J. Roos, and S.J.M.H. Hulscher. Process-based modelling of bank-breaking mechanisms of tidal sandbanks. *Continental Shelf Research*, 167:139–152, 2018. doi: 10.1016/j.csr.2018.04.007.
- T. Verwaest, R. Delgado, J. Janssens, and J. Reyns. Longshore sediment transport along the Belgian coast. 04 2011. doi: 10.1142/9789814355537_0115.
- M. Walgreen, D. Calvete, and H.E. de Swart. Growth of large-scale bed forms due to storm-driven and tidal currents: a model approach. *Continental Shelf Research*, 22:2777–2793, 2002. doi: 10.1016/S0278-4343(02)00126-7.

- B. Yuan and H.E. de Swart. Modeling the finite-height behavior of offshore tidal sand ridges, a sensitivity study. *Marine Geology*, 390:199–213, 2017. doi: 10.1016/j.margeo.2017.07.005.
- B. Yuan, H.E. de Swart, and S.J.M.H. Panadès. Modeling the finite-height behavior of offshore tidal sand ridges, a sensitivity study. *Continental Shelf Research*, 137:72–83, 2017. doi: 10.1016/j.csr.2017.02.007.
- J.T.F. Zimmerman. Dynamics, diffusion and geomorphological significance of tidal residual eddies. *Nature*, 290:549–555, 1981.